Light Stable Isotopic Compositions of Enriched Mantle Sources:

Resolving the Dehydration Paradox

Jacqueline Eaby Dixon[1], Ilya Bindeman[2], Richard Kingsley[3], Kyla Simons[4], Petrus LeRoux[5], Tina Rau Hajewski[6,#], Peter Swart[7], Charles Langmuir[8], Jeffrey Ryan[9], Kristina Walowski[2,*], Ikuko Wada[10], Paul Wallace[2]

[1]College of Marine Science
University of South Florida
140 Seventh Ave. South
St. Petersburg, FL 33701

[2]Department of Earth Sciences
University of Oregon
1275 E. 13th Ave
Eugene, OR 97403-1272
USA

[3]Graduate School of Oceanography
University of Rhode Island
215 South Ferry Road
Narragansett, RI 02882-1197

[4]Exxon-Mobil
Houston, TX
USA

[5]Department of Geological Sciences
University of Cape Town
Rondebosch, 7700
South Africa

[6]Department of Geology
University of Miami
Miami, FL 33146
USA

[7]Division of Marine Geology and Geophysics
Rosenstiel School of Marine and Atmospheric Science

University of Miami
4600 Rickenbacker Causeway
Miami, FL 33149
USA

[8]Department of Earth and Planetary Science
Harvard University
20 Oxford Street
Cambridge, MA 02138

[9]School of Geosciences
University of South Florida
4202 E. Fowler Ave., NES 107
Tampa, FL 33620-5550
USA

[10]Department of Earth Sciences
University of Minnesota
310 Pillsbury Dr. SE
Minneapolis, MN 55455-0231

#now at University of Iowa Hospitals & Clinics
200 Hawkins Dr
Iowa City, IA 52242

*now at Department of Geology
Middlebury College
Middlebury, VT 05753

Contents of this file

INTRODUCTION

Supplementary text S1 presents analytical techniques for analysis of water concentrations (FTIR and TC/EA) and isotopic ratios of hydrogen (Conventional and TC/EA), boron (laser ablation ICP-MS), lithium (MC-ICP-MS) and oxygen (laser fluorination). Of special significance, we performed an interlaboratory comparison between conventional and TC/EA techniques for hydrogen isotopic ratios in basaltic glasses, resulting in revisions to the TC/EA method.

Supplementary text S2 presents descriptions of sample location and provenance, regional geochemical trends, and shallow modification of volatiles by degassing or assimilation for each study region.

Supplementary text S3 presents additional light stable isotope data that is available for several of the study areas.

Supplementary text S4 describes the procedures used to estimate mixing end members and calculate mixing curves.

Supplementary Table S5 summarizes acronyms.

S1. ANALYTICAL TECHNIQUES

S1.1 Dissolved Water and Carbon Dioxide Concentrations by Fourier-Transform Infrared Spectroscopy

Dissolved water and carbon dioxide concentrations in glasses were measured using transmission infrared spectroscopy, following the procedures of *Dixon and Clague* [2001]. New data are presented for the Arctic ridges, along with published values from the Azores Platform, south Atlantic, and the Easter Microplate – Salas y Gomez Seamount Chain (EMP-ESC) system [*Dixon et al.,* 2002; *Simons et al.,* 2002]. Glass chips were doubly polished to a thickness between 300 and 1000 microns. Infrared transmission spectra in the 4000 to 1200 cm^{-1} (2.5 to 8.3 μm) range were collected at the University of Miami using an infrared microscope attachment to a Brüker IFS-66 FTIR spectrometer, with Globar source, KBr beam splitter, HgCdTe detector, and mirror velocity of 1.57 cm/s. Spot sizes were typically 200 μm in diameter, with aperture size selected to avoid devitrified zones. Typically, 1012 scans were collected for each spectrum. Total H_2O was determined on the raw absorbance spectrum using a flat-line background correction. H_2O concentrations were derived from the spectra using Beer-Lambert law calibration (see review in *Ihinger et al*. [1994]). The thickness, or path length, was measured with a digital micrometer with a precision of ±1-2 μm. Glass density was assumed to be 2800 kg/m^3. A molar absorptivity of 63 ± 3 l/mol-cm was used for total dissolved water using the fundamental OH stretching band at 3535 cm^{-1}. Precision of the analyses is about ±2 % for total water. The accuracy of the total water analyses is about ± 10 %, the same as reported by *Dixon et al*. [1991].

S1.2 Hydrogen Isotopic Compositions by Stepped-heating Manometry/Mass Spectrometry

Glasses from the Arctic and South Atlantic [*this study*], as well as from the EMP-ESC system [*Kingsley et al*., 2002], were analyzed for δD_{SMOW} using stepped-heating manometry/mass

spectrometry at the University of Miami Stable Isotope Laboratory following the procedures of *Kingsley et al*. [2002]. This method, also referred to as "conventional", is similar to that used by most earlier studies of oceanic basalts, including *Poreda et al*. [1986], *Kyser and O'Neil* [1984], *Pineau and Javoy* [1994], *Cartigny et al.,* 2008, and *Clog et al*. [2013].

Hand-picked glass chips 1 to 5 mm in diameter and weighing 0.25 g to 3.0 g depending on water concentration are placed into an outgas furnace for stepped-heating. Prior to each heating step, samples are exposed to oxygen from O_2 desorbed from a molecular sieve in the extraction line to provide an oxidizing atmosphere during extraction. Samples are then brought to a prescribed temperature and allowed to degas for 30 min at each step (600–800°C and 800–1000°C), or in some cases at a single step of 700–1000°C. These increments are selected because the bulk of the water (>95%) in tholeiitic glasses is exsolved during the 800–1000°C heating step [*Kingsley et al.,* 2002]. This is consistent with several other studies [e.g., *Kyser and O'Neil*, 1984], where water liberation was found to peak at 900°C ± 50°C. Also, the choice to measure only these steps was made in order to minimize the effect of adsorbed water released at low temperatures and to minimize the effect of variable amounts of water in microvesicles affecting the D/H measurement.

After 30 minutes, all gasses liberated during a particular heating step are transferred through the extraction line, and CO_2, SO_2, and H_2O are condensed in a liquid nitrogen (LN_2) cold trap at -195°C. The CO_2 (saved for isotopic measurements) and SO_2 (discarded) are selectively separated from H_2O by warming the cold finger to -130°C (with a mixture of LN_2 and pentane) and to -75°C (with a mixture of LN_2 and methanol), respectively. The cold trap is then heated to >100°C, and the pressure of the water vapor is measured using a capacitance manometer to determine whether there is enough water vapor present to measure in the mass spectrometer. If so, the water vapor is then reacted with uranium metal to produce pure hydrogen gas. The H_2 is transferred to a sample vessel using a Toepler Pump (mercury-ram pump) and then removed from the extraction line and placed on the mass spectrometer for measuring D/H. Experiments presented in *Kingsley et al.* [2002] revealed that where more than one temperature step contained enough water to measure, the lower temperature step (e.g., 600-800°C) contained hydrogen with a lower δD_{SMOW} value (i.e., lighter) than the hydrogen liberated at 800–1000°C, with the isotopic difference averaging around -20 ‰ (see Figure 3 in *Kingsley et al.* [2002]). This is consistent with the results of *Kyser and O'Neil* [1984] in their step-heating experiments of MORB glasses and will be discussed in more detail below (section S1.5). In cases where significant amounts of water were liberated in more than one step, the value taken to represent the δD_{SMOW} value of magmatic hydrogen in the basaltic glasses was calculated using a weighted average based on the pressures (atomic mass 2) of the two aliquots measured on an equal volume basis at the inlet of the mass spectrometer. Three glasses analyzed with the above method and by *Poreda et al*. [1986] at Scripps Institution of Oceanography agree within ±3 ‰.

The new δD_{SMOW} analyses reported here were measured over a decade (1997 – 2006) and conditions were not identical over that time period. To reduce systematic offsets between data generated at different times, we re-examined the normalization process to SMOW standards run as unknowns during the analytical sessions, resulting in small corrections as described below.

The Arctic Ridges samples [*this study*] were run in 2005 and were corrected to SMOW aliquots run during that time with the correction being +10.4 ‰ ± 1.7 (n = 5). This was the mean of 5 runs of SMOW aliquots run during the same period. The mass-spectrometer used during 2005 and 2006 was a different model (Finnigan Delta Plus) rather than a Finnigan 251 used earlier. The South Atlantic samples [*this study*] were run in 1998 and in 2006. The 1998 samples were analyzed on a Finnigan 251 mass-spectrometer. These analyses were not normalized to the measured SMOW aliquots because the pressure-corrected values for the SMOW runs was only about +1.5 ‰. The samples run in 2006 were run on a Finnigan Delta Plus and were corrected to SMOW because the SMOW aliquots gave +11.0 ‰ ± 2.2 (n = 5).

The EMP-ESC δD_{SMOW} analyses [*Kingsley et al.,* 2002] were measured during 4 intervals: 1997, 1998, 1999, and 2000. During 1998 and 1999, there was a well-understood pressure dependency on the mass-spectrometer measurements. Most Easter glasses were reanalyzed during one period in 2000, though the older data are still reported in *Kingsley et al.* [2002]. In 1997, the standard gas used was a -120 ‰ versus SMOW gas. EMP-ESC glasses run at this time (GL07 D53-2g, GL07 D43-1g) were not corrected to SMOW aliquot runs, which gave an average of +4.3 ‰ at the time. In 1998 and 1999, the standard gas was a 0 ‰ versus SMOW gas. During this period, there was an obvious pressure-dependence on the D/H value given by the mass-spectrometer. These EMP-ESC glasses were not corrected for aliquots of SMOW run during the time, but the pressure corrected values for SMOW aliquots were close to zero (+1.5 ‰). In the 2000 analytical sessions, the standard gas was a 0 ‰ gas, so a SMOW correction was not needed. These samples were just zero corrected, as were all the others in the previous periods, and were not corrected for SMOW aliquot runs. The values for SMOW aliquots run during this time were an average of +6.3‰ and ranged from +1.5 ‰ to +11.8 ‰.
For this study, we have made small corrections (up to -6 ‰) to the previously reported Easter data [*Kingsley et al.,* 2002] to consistently normalize to SMOW for each analytical run. These corrections were not applied in *Kingsley et al.* [2002] because 1) the magnitude of the corrections was reflected in the ± 5 ‰ error estimate; 2) accuracy of SMOW aliquots was not well known; and 3) it was consistent across all samples to just correct for the zero offset on each day.

The formula for calculating the reported values is:

$$\partial D\%_{(SA-SMOW)} = \left[\left(\frac{\partial D\%_{(SA-SG)} - 1000}{\partial D\%_{(SMOW-SG)} - 1000} \right) - 1 \right] \times 1000$$

where *∂D‰(SA-SMOW)* is the value of the sample relative to SMOW (the value we report), *∂D‰(SA-SG)* is the value of the sample relative to the standard gas and is the value measured on the mass spectrometer, and *∂D‰(SMOW-SG)* is the value of the SMOW runs relative to the standard gas. For the EMP-ESC samples, this value was zero. For the runs in 2005 and 2006 (on the Delta Plus) this value was the one reported above for aliquots of SMOW run during this time (+10.4 ‰ for 05 and +11.0 ‰ for 06). Corrections to previously published data are listed in Table S1-1.

S1.3 Water Concentrations and Hydrogen Isotopic Analysis by TC/EA

The water content and hydrogen isotope ratio of glasses from the Azores Platform and EPR 6° to 17°N were measured by continuous flow via the High Temperature Conversion / Elemental

Analyzer (TC/EA) technique at the University of Oregon. This technique includes a gas chromatography (GC) column (5 Å molecular sieve, 80-100 mesh, 0.6 long and 0.4 mm inside diameter) coupled to a Thermo Scientific MAT253 mass spectrometer. The use of a higher acceleration voltage and larger radius instrument allows us to analyze samples one quarter the size of that required for more common but less sensitive TC/EA - Delta V systems, with water contents as low as 0.1 wt%. Glass chips are crushed and sieved into <50µm, 50-100µm, 100-250 µm, 250-500 µm, 500-1000 µm, and 1000-2000 µm size fractions in order to test the grain size effect on the results. Fractions are examined under transmitted and reflected light in milligram quantities assuring good quality of the concentrate. Crystal-poor glass chips with no visible clay minerals are handpicked under the microscope. In glasses containing crystals too small to be separated from the matrix, modal proportions are estimated and used to correct the measured water contents (Table S1-2). Glasses are dried in a vacuum oven at 110°C-220°C for 2 hours before loading into silver foil cups (1-10 mg of glass depending on water content). The silver foil cups are wrapped around the glasses and placed in the vacuum oven overnight for 12-15 h at ~130°C to remove surface moisture, as capsules are not welded and water can escape freely. Silver cups are then transferred to a carousel autosampler on the TC/EA over ~10 min, and purged with pure He gas for 1-2 h before analyses. Each sample is dropped into a high temperature furnace (1450 °C), requiring ~6 minutes per analysis. All water related to loaded glass is analyzed by instantaneous extraction, without any step heating. Under the He carrier gas, water reacts quickly with hot vitreous C to produce CO and H_2 gases that are separated by the GC column. These flow to a Thermo Scientific Conflow III, which lowers the sample pressure to atmospheric and meters pulses of reference gas, and then to the mass spectrometer for hydrogen isotopic ratios and H_2O content measurements via mass 2 and 3 peak integration. The H3 factor (formation of 3 hydrogens together inside the mass spectrometer source) is determined by varying pressure in the beginning of each session and a correction measuring a few permil is applied to all samples run on that day. 1% H_2 gas in a 99% He tank is used for reference gas calibration. Typically we run 3 to 4 peaks of on-off standard gas before the unknowns and 1 peak after the unknown.

Total (>95%) water extraction from analyzed basaltic glasses is documented in Figure S1-3, comparing FTIR analyses and manometry measurements with TCEA data. Because extraction and conversion to H_2 gas proceeds at 1450°C, D/H isotopic fractionation between remaining water (if any) and extracted water is likely to be minimal and cannot explain differences between methods described below.

In order to convert measured D and H peak areas into ratios on a SMOW scale, samples are always run against 3 to 4 sets of 3 standards covering the D/H of the unknowns, interspersed with the unknowns during each analytical session, enabling 3-point calibration.

Samples initially run during 2012 to 2014 analytical sessions were calibrated with three mica standards that span the range of the expected sample isotopic compositions: internationally known NBS30 biotite (δD = -65.7 ‰, H_2O = 3.5 wt. %), and two in-house standards calibrated with the NBS30 (RUH2 white mica, δD = -98.2 ‰; H_2O = 4.5 wt. % and Butte MT biotite, BUD, δD = -161.8 ‰; H_2O = 2.8 wt. %). However, recent work by *Qi et al.* [2014] demonstrated that the D/H value for the NBS30 biotite mica standard, used for decades in many labs for calibration purposes, was likely incorrect due to heterogeneity not fully explored in the three analyses used to determine the reference values [http://wwwpub.iaea.org/MTCD/publications/PDF/te_825_prn.pdf, page 20 -21]. When we analyzed NBS30 by TC/EA versus standard waters sealed in Ag cups following the method of

Qi et al. [2010], we did not reproduce the reference value of -65.7 ‰, but instead determined values heavier by 15 to 21 ‰ (mean +16 ‰). After reevaluation of NBS30, the mica standard values obtained and used in this study are NBS30 δD = -50.0 ‰, RUH2 δD = -81.4 ‰ and BUD δD = -144.7 ‰ (Table S1-2). Ongoing cross-calibration of two new USGS mica standards (USGS 57 and 58) that are proposed to replace the exhausted NBS30 supply made by the Univ. of Oregon and four other labs, confirms this result (publication pending, http://isotopes.usgs.gov/lab/referencematerials.html).

Based on reevaluation of the mica standard values, some of the volcanic glasses were later run directly against international standard waters: V_{SMOW} (δD = 0 ‰); GISP (δD = -189.7 ‰), and Lake Louise (δD = -150.2 ‰) that cover the range of the unknowns, as well as NBS30 and other mica standards. When run against these waters, the 3-point calibration was applied to the unknown glasses, and the raw SMOW water value typically comes within a few permil of a nominal 0 ‰ value. Different analytical sessions will differ in D/H raw output of water standards by a few permil due to variable instrumental mass fractionations, which results from several factors including flow rate, H3 factor, condition of the CONFLOW shifted unknown, and values of the reference gas.

Herein we report all of our δD data relative to water standards spanning the δD range of the glass unknowns, but we use NBS30 to calibrate $[H_2O]_{tot}$ in our glass samples. We obtained the following conversion equation between our mica standards and four water standards run in 7 different analytical sessions: y = 0.989x + 15.38 (R^2 = 0.992). As it is very nearly a linear relation, we are confident in our systematic +16 ‰ correction applied to our data for samples initially calibrated to the NBS30 (e.g. Macquarie Ridge glasses [*Bindeman et al.,* 2012]). We also ran other silicate glasses previously measured by a conventional method using a SMOW standardization from *Newman et al.* [1988]. Comparable δD and total water contents were obtained by the TC/EA method in the Univ. Oregon Lab and the Reston USGS Lab (Table S1-2). Complete water extraction from both solid materials (micas and glass) and complete conversion of the extracted water to hydrogen has been demonstrated. In one test, the isotopic composition of V_{SMOW} sealed in Ag tubes was measured at furnace temperatures of 1400 and 1450°C with intensity >1000mV. No variations in δD are observed between the two different temperature conditions (Figure S1-1).

The reproducibility and precision of the isotopic composition was investigated as a function of the spectrometer signal amplitude by analyzing a range of weights of the standard RUH2 (0.1 mg to 3 mg; Figure S1-2A). The signal amplitude directly depends on the quantity of extracted water, as shown by the good linear correlation (R^2=0.98) between the amount of standard and the amplitude of the signal measured on mass 2. Signal intensities higher than 1000-1500 mV lead to very reproducible δD measurements (δD ± 1.3 ‰; 2 std. error). Lower sample mass and thus lower water yield leads to less reproducible and potentially heavier δD (Figure S1-2B). Analyses with mass 2 intensity ≤ 500mV exhibit the greatest analytical errors (±7.4 ‰ on δD; 2 std. error) with potential shift +20 ‰ relative to those at higher amplitude. For >1000 mV intensity on mass 2, raw δD values are very reproducible with a δD = 7.28 ± 0.52 ‰ (Figure S1-2) relative to the reference gas (1 % H_2 in He). Note that samples ran against V_{SMOW} (sealed in Ag-capsules, as suggested by *Qi et al.* [2014]) required a 6 ‰ to 8 ‰ correction (7.3 ‰ in Figure S1-2) and are similar for the other waters. All samples analyzed with the TC/EA method should be loaded in quantities appropriate to generate signal on mass 2 above 1500 mV.

S1.4 Water Concentration FTIR and TCEA Interlaboratory Comparison

Figure S1.3 shows water concentrations in Mid-Atlantic Ridge and Easter Microplate – Easter Salas y Gomez Seamount Chain glasses measured by FTIR [*Dixon et al.*, 2002; *Simons et al.,* 2002] and by TC/EA (this study). Water concentrations measured by FTIR and TC/EA on the Azores Platform and EMP-ESC glasses show excellent agreement. For H_2O concentrations < 1 wt. %, the slope of the non-weighted least square regression fit indicates that the TC/EA data are slightly lower than FTIR data by ~ 4 %, however the slope is not different from unity at the 2σ level (Figure S1-3). Excellent agreement between the techniques indicates efficient extraction (~96%) by TC/EA technique. Any offset in the δD_{SMOW} values, discussed below, is unlikely to be due to incomplete water extraction during TC/EA analysis.

S1.5 Hydrogen Isotopic Stepped-Heating Manometry – TC/EA Interlaboratory Comparison

Four Easter Microplate – Easter Salas y Gomez Seamount Chain glasses, previously analyzed for hydrogen isotopes by stepped-heating manometry/mass spectrometry [*Kingsley et al.,* 2002], were selected for analysis by TC/EA. Comparison of the new standard water calibrated TC/EA data (+16 ‰ relative to earlier mica-calibrated data) with the SMOW-normalized conventional data shows the TC/EA data lighter by 10 ± 6 ‰ (Figure S1-4). This remaining offset most likely reflects the difference in temperature intervals over which water is collected between the two techniques. *Kingsley et al.* [2002] showed that >95% of the water is extracted above 700°C. The remaining 5% of water extracted between 150 and 700°C, excluded from conventional but included in TC/EA analysis, would need to be extremely light (δD_{SMOW} of ~-200 ‰) to explain the observed offset. Assuming that the different treatment of the low temperature fraction is the cause of the offset, there are two possibilities. The low temperature water could be either magmatic, implying that the conventional analyses are missing a magmatic component, or non-magmatic, implying that the TC/EA analyses contain some form of contamination. In the former case, stepped-heating during extraction shows that hydrogen extracted at a lower temperature step (e.g., 600-800°C) is typically lighter than that liberated at the higher temperature step (e.g., 800–1000°C) with the isotopic difference averaged around -20 ‰ (see Figure 3 in *Kingsley et al.* [2002]). This is consistent with the results of *Kyser and O'Neil* [1984] in their step-heating experiments of MORB glasses. This trend is not consistent with preferential extraction at lower temperatures of heavier dissolved molecular water relative to OH- groups [*Newman et al.,* 1988] or of heavier microvesicles [*Kyser and O'Neil,* 1984; *Pineau and Javoy*, 1994], but is consistent with preferential extraction of H over D during heating [*Kyser and O'Neil*, 1984]. In this case, conventional analyses would have excluded this small fraction of light hydrogen and should be adjusted to lighter values. The latter possibility asserts that the low temperature light-H fraction is related to the preferential extraction of isotopically light alteration minerals (e.g., clays, zeolites [*Sheppard and Gilg*, 1996]) or surface absorbed H_2O, which would be required to have remained in the glass after drying at 150°C but be removed during step-heating to 700°C. If this were the case, the TC/EA data would include low-T contamination and should be adjusted to heavier values. Arguments against this are that glasses in both techniques were hand-picked to avoid alteration phases and the smaller volume of glass used in TC/EA analysis (a few milligrams as opposed to hundreds of milligrams) makes it less likely for alteration phases to slip through visual inspection of glass grains. More work is required to better quantify the origin of the offset between the two techniques.

S1.6 Boron Isotopic Compositions by laser ablation ICP-MS (South Atlantic glasses)

In situ boron isotopic compositions were measured by laser ablation, multiple-multiplier ICP-MS at the Department of Terrestrial Magnetism, Carnegie Institute of Washington following *le Roux et al.* [2004]. This technique avoids sample chemistry and achieves high enough ion yield to obtain better than 1 ‰ precision (2 σ) on even low boron abundance glasses (as low as 0.39 ppm B). It also permits correction of the high mass fractionation produced by the ICP-MS (100-150 ‰ for measured $^{11}B/^{10}B$ ratios) to better than 1‰ absolute accuracy by sample-standard switching. In addition to eliminating the need for chemical separation for boron, the technique has low instrument memory and background (<300 cps compared to >100 000 cps for solutions), high sensitivity, requires small sample size, and gives precise spatial control on material analyzed.

S1.7 Lithium Concentrations and Isotopic Compositions by MC-ICP-MS (Azores glasses)

Lithium was measured by MC-ICP-MS at Lamont-Doherty Earth Observatory using chemistry and column procedures following *Tomascak et al.* [1999], with minor modifications. This chemistry is based on the efficient separation of Li from other interfering elements (particularly Na) using a cation exchange resin and a mixture of nitric acid and methanol to maximize separation. This method was first studied by *Strelow et al.* [1974] and has been the basis of the chemistry of many other groups [*Moriguti and Nakamura*, 1998; *Nishio and Nakai*, 2002; *Pistiner and Henderson*, 2003; *Ryan and Kyle*, 2004; *Tomascak et al.*, 2008]. We modified the original column procedure of *Tomascak et al.* [1999] to include a second column, ensuring that the sample was as clean as possible, and to further separate Na from Li if necessary. A complete review of chemistry and procedures can be found in Appendix B of *Simons et al.* [2010].

S1.8 Oxygen Isotopic Compositions (Arctic glasses)

Oxygen isotopes from Arctic ridge samples were measured by J. Eiler at the California Institute of Technology between 6/30/2005 and 7/12/2005. The laser-fluorination technique used is described in *Cooper et al.* [2004].

The interlaboratory standard garnet UWG-2 was used as a normalizer to the unknown MOR glasses. For the nine-day period in which these glasses were analyzed for oxygen isotopes, the garnet standard was also run and measured a $\delta^{18}O_{SMOW}$ of 5.932 ± 0.080 (1 s.d., n = 9) taken as the precision of the method. We used the accepted value for this standard garnet of 5.800 to normalize all the unknown glasses. This was done on a daily basis (i.e. the unknowns were normalized to the average of three to six UWG-2 runs of that particular day). These corrected values are reported here.
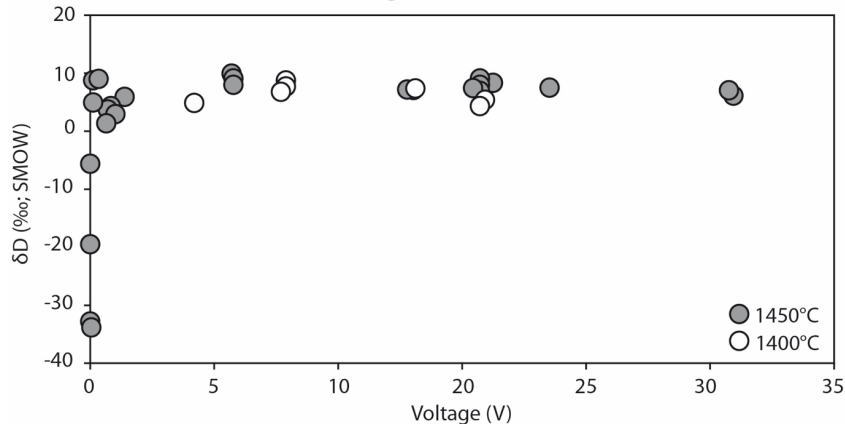
Figure S1-1. H isotopic composition of V_{SMOW} at 1400 and 1450 °C on the TC/EA as a function of sample size and water concentration. Intensity is measured on mass 2. For intensity > 1000 mV, raw δD = 7.28 ± 0.52 ‰ (from *Martin et al.* [2017]).
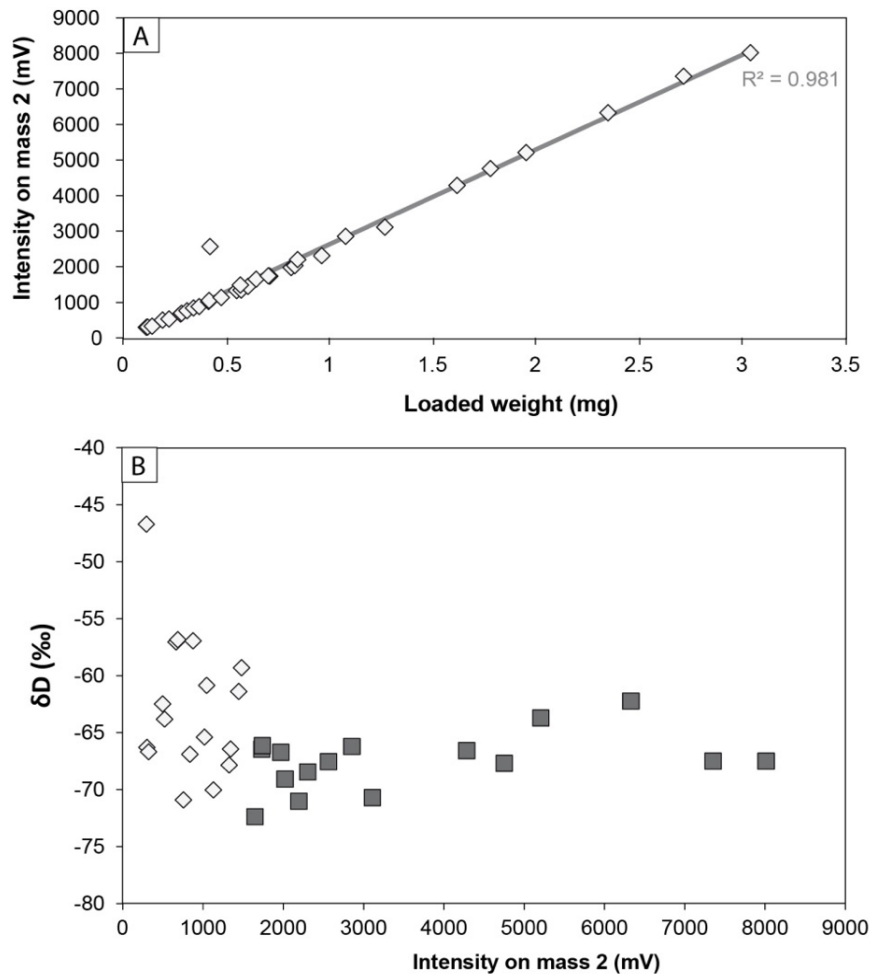
Figure S1-2. A) Correlation between weight of mica standard RUH and intensity measured on mass 2 of MAT253 mass spectrometer. B) δD measured and not corrected on RUH2 as a function of intensity measured on mass 2. Open and closed symbols highlight 1500 mV limit. Reproducibilities are: ≤ 500 mV: -61.2 ± 7.4 ‰; 500 mV to 1000mV: -61.5 ± 4.5 ‰; 1000 to 1500 mV: -62.7 ± 2.9 ‰; >1500 mV: -67.5 ± 1.3‰. From *Martin et al.* [2017].
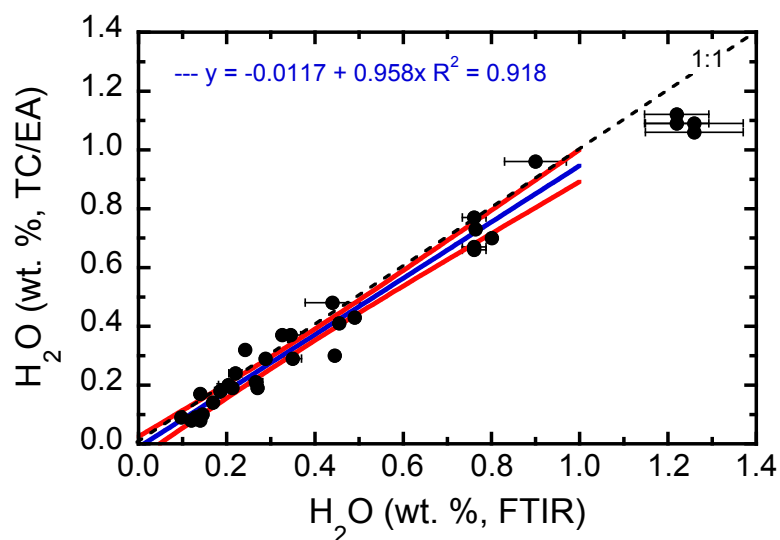
Figure S1-3: Comparison of H_2O concentrations measured by FTIR or manometry and TC/EA on basaltic glasses from the Azores Platform Easter Microplate and Easter Salas y Gomez Seamount Chain. Dashed line is 1:1 line. Blue line is the non-weighted least square regression fit for H_2O concentrations < 1 wt. %. Red curves are 2σ. The slope is not different from unity at the 2σ level. When data with larger uncertainties > 1 wt. % are included, TC/EA lower than FTIR data by ~10% (regression fit is y = 0.0079 + 0.896x, R^2 = 0.974). Larger uncertainties FTIR analyses of high H_2O glasses are primarily due to glass heterogeneity.
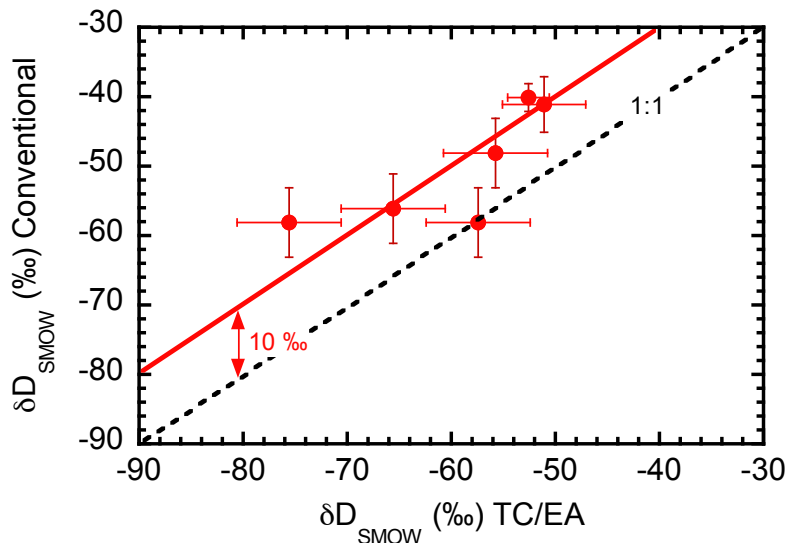
Figure S1-4. Comparison of δD_{SMOW} values measured by conventional stepped-heating manometry/mass spectrometry and TC/EA calibrated to standard water references. Remaining 10 ± 12 (2σ) ‰ offset is likely related to different treatment of low T light hydrogen, which is excluded in conventional analysis and included in TC/EA.

Table S1-1	Run date	δD Kingsley et al. [2002]	SMOW Correction (‰)	δD SMOW Adj. (‰)	TC/EA value (± 2 σ)
GL07 D53-2g	1997	-54	-4	-58	-57.5 ± 3.5
GL07 D43-1g	1997	-44	-4	-48	-55.9 ± 3.6
GL07 D30-1g(a)	1998/1999 600-1000°C	-42	-1	-43	
GL07 D30-1g(b)	2000 700-1000°C	-37	-6	-43	
GL07 D46-2g(a)	1998/1999 650-1000°C	-51	-1	-52	
GL07 D46-2g(b)	2000 600-1000°C	-44	-6	-50	
GL07 D48-4g(a)	1998/1999 600-1000°C	-40	-1	-41	-52.7 ± 4.8
GL07 D48-4g(b)	2000 700-1000°C	-33	-6	-39	"
GL07 D50-1ag	1998/1999	-41	-1	-42	
GL07 D51-3g	1998/1999	-52	-1	-53	
GL07 D56-2g	1998/1999	-47	-1	-48	
EN113 4D-1Ag	1998/1999	-55	-1	-56	-
EN113 5D-1Ag	1998/1999	-49	-1	-50	-
EN113 6D-1A(a)	1998/1999	-38	-1	-39	-51.1 ± 5.4
EN113 6D-1A(b)	2000	-37	-6	-43	"
EN113 7D-1g	1998/1999	-43	-1	-44	-
EN113 24D-1Ag	1998/1999	-57	-1	-58	-75.7
EN113 26D-1g	1998/1999	-63	-1	-64	-
EN113 35D-1g	1998/1999	-57	-1	-58	-
EN113 36D-1g	1998/1999	-59	-1	-60	-
GL07 D32-4g	2000	-43	-6	-49	-
GL07 D42-1g	2000	-36	-6	-42	-
GL07 D47-2g	2000	-41	-6	-47	-
GL07 D52-5g	2000	-51	-6	-57	-
EN113 41D-1g	2000	-50	-6	-56	-65.7 ± 4.8
EN113 30D-1(a)	2000	-40	-6	-46	
EN113 30D-1(b)	2000		-6		
mean offset ($\delta D_{conv} - \delta D_{TC/EA}$)					10 ± 12

Table S1-1. Correction factors used for conventional δD data using data from *Martin et al.* [2017].

RHYOLITES	U. Oregon					Reston USGS Lab, 2015			
	δD ‰	std	n	H_2O wt%	std	δD ‰	std	H_2O wt%	std
MC84-1 (-75 ‰, 0.78 %)[^]									
UO grain size									
149–250 µm	-74.6	2.0	3	0.75	0.01	-75		0.7	
50–250 µm	-71.5	2.4	3	0.75	0.00	-71		0.8	
Upper Dome NW Coulee (-104 ‰, 0.28 %)[^]									
149–250 µm	-103.6	0.2	2	0.28	0.01				
50–250 µm	-101.8	3.6	2	0.27	0.01				
NE tip N lobe of Northern Coulee (-107 ‰, 0.27 %)[^]									
149–250 µm	-103.8	16.1	3	0.09	0.03				
50–149 µm	-99.5	9.8	3	0.09	0.01				
IDDP rhyolitic glass (-118‰, 1.80% and 1.77±0.14 by FTIR)[#]	-114.2	1.83	9	1.83	0.07				
BASALTS									
GL07-D48-4 (-37 ‰, 1.26 %)									
149–250 µm	-39.7	0.4		1.13	0.01	-40		1.10	
50–149 µm	-37.1	0.2		1.13	0.00	-37		1.10	
MICA STANDARDS run vs water	1 std		n				std	n	
NBS30*	-50.0	3.2	22	3.5	0.06	-50.6	4.9	6	*
RUH2	-81.4	2.9	30	4.3	0.03	-84.0	1.4	2	4.50 0.0

Table S1-2. δD and total water measured in samples run previously by conventional methods and standardized differently. Rhyolites are original samples from *Newman et al.* [1988] and *Zierenberg et al.* [2013] (sample names and values in bold font). Basalt sample (GL07-D48-4) from *Kingsley et al.* [2002]. Samples analyzed in Reston USGS lab by H. Qi.

S2. SAMPLE LOCATIONS, PROVENANCE, REGIONAL GEOCHEMICAL TRENDS.

S2.1 Global Sample Distribution
Locations of all samples are shown in Figure S2-1.

S2.2 Radiogenic Isotopic and Trace Element Compositions of all samples in this study.

Throughout this study, we use high $^{87}Sr/^{86}Sr$, low $^{206}Pb/^{204}Pb$, and high Ba/Nb as indicators of an EM-type source, and low $^{87}Sr/^{86}Sr$, high $^{206}Pb/^{204}Pb$, and low Ba/Nb as indicators of a PREMA-type source. Data for all samples included in this study are shown in Figures S2-2 and S2-3 to facilitate comparison of different regions.

S2.3 Arctic Ridges

<u>Sample Locations and Provenance:</u> The Mid-Atlantic Ridge north of Iceland is composed of three major ridge segments (Figure S2-4). From north to south, these are the Knipovich, Mohns, and Kolbeinsey ridges. Jan Mayen Island is located between the Kolbeinsey and the Mohns Ridges. Fresh MORB glasses from the URI collection of J.-G. Schilling include 54 sampling sites separated by 30 ± 20 km. These samples have been previously analyzed for major and trace elements, radiogenic isotopes (Sr, Nd, Pb, and Hf), and noble gases [*Sigurdsson*, 1981; *Schilling et al.*, 1983; *Neumann and Schilling*, 1984; *Poreda et al.*, 1986; *Mertz et al.*, 1991; *Devey et al.*, 1994; *Haase* et al., 1996; *Mertz and Haase,* 1997; *Schilling et al.*, 1999].

<u>Regional Geochemical Trends:</u> The dominant geochemical feature along the Arctic Ridges is the long-wavelength contribution of the Jan Mayen plume, manifested as a mixing gradient in radiogenic isotopes and trace element ratios and concentrations of basalts from 72° to 74°N along the Mohns ridge (Figure S2-5) [e.g., *Schilling et al.,* 1999]. South of Jan Mayen Plateau, the Spar Fracture Zone separates Iceland-influenced from Jan Mayen-influenced basalts. Basalts from the Knipovich Ridge are more heterogeneous, most likely related to extremely slow-spreading bordering the Svalbard continental shelf. Scatter in Mohns and Knipovich basalts represents smaller scale heterogeneities superposed on the longer length scale Jan Mayen plume signal.

Though significantly depleted in incompatible elements, the depleted Mohns Ridge depleted end-member has elevated $^{87}Sr/^{86}Sr$ and elevated Ba/Nb at unradiogenic $^{206}Pb/^{204}Pb$, consistent with contamination of the ambient NMORB mantle in the region by a dispersed EM-type mantle component. Compositions of the Arctic Ridge basalts can be modeled by pseudo-binary mixing between two end-members – PREMA, and DMM+EM.

Basalts from the Arctic Ridges are distinctive for two reasons. First, all basalts have low $^{3}He/^{4}He$ signature, eight or less (Figure S2-5) [*Poreda et al.,* 1986], suggesting a lack of involvement of the high $^{3}He/^{4}He$ Icelandic plume or other lower mantle sources. Second, the basalts are generated by relatively low extents of partial melting. The mean degree of melting decreases by a factor of 2 to 3 from 67°N on Kolbeinsey Ridge to 78°N on Knipovich Ridge, as the half-spreading rate decreases from 1.0 to 0.6 cm/yr [*Waggoner,* 1990; *Schilling et al.,* 1999]. These low extents of partial melting, particularly in the vicinity of the Jan Mayen platform, result in additional enrichments in incompatible elements and increases in ratios of highly

incompatible to less incompatible elements, such as La/Sm, H_2O/Ce, and K_2O/TiO_2, and to a lesser degree Ba/Nb

In this study, we present new H_2O, δD_{SMOW} (conventional) and $\delta^{18}O$ for Arctic Ridge basalts. $\delta^{18}O$ data are reported in S3.1 below. Water concentrations in Arctic Ridge glasses (0.2-1.8 wt. %) are consistent with previously reported values [*Michael,* 1995]. Most of the Jan Mayen glasses were of insufficient quality for FTIR analysis due to devitrification during degassing. FTIR analysis was successful for the one low K_2O Jan Mayen sample, EN026-7D-1. Water concentration in this glass (0.8 wt. %) is consistent with the values in the highest ^{206}Pb/^{204}Pb Mohns Ridge basalts, suggesting that this sample has not suffered degassing-related H_2O-loss.

H_2O behaves incompatibly during mantle melting and subsequent shallow differentiation processes [e.g., *Michael,* 1995]. Comparison of H_2O to other incompatible elements in oceanic basalts has shown that its behavior during melting and crystallization is similar to La, Ce, or K, with perhaps the greatest similarity to Ce [*Dixon et al.,* 1988; *Michael,* 1988, *Jambon and Zimmermann*, 1990, *Michael*, 1995]. Positive correlation between H_2O and Ce for Arctic glasses (Figure S2-6), indicates minimal shallow degassing or assimilation modification of these samples, and is similar to that observed in Azores Platform basalts (Figure S2-10).

δD_{SMOW} range from a typical MORB value of -78 ‰ near the Spar Fracture Zone on the Kolbeinsey Ridge to a deuterium-enriched high of -29 ‰ on the Knipovich Ridge (Figure S2-7). The binary mixing relationship along the Mohns Ridge defined on the basis Pb-Sr-Nd-Hf isotope ratios is also present in the D/H variation, grading from the Jan Mayen platform (PREMA-type, with the highest δD_{SMOW} (-33 ‰) eastward to the Greenland Fracture Zone, where values of around -60 ‰ are observed.

Shallow Modification: There is no evidence for degassing of water from Arctic Ridge basalts, with the exception of the basalts close to Jan Mayen. However, degassing-devitrification made those samples unsuitable for FTIR or hydrogen isotopic analysis.

S2.4 Azores Platform Basalts

Sample Location and Provenance: The Azores Platform samples were dredged by the *R/V Atlantis II* on the 1992 French American Zaps and Rocks (FAZAR) expedition [*Langmuir et al., 1992*]) between 33.2° and 40.5°N, with depths varying between 926 and 3,900 m (Figure S2-8).

Regional Geochemical Trends: The dominant long-wavelength geochemical and bathymetric anomaly (Figure S2-9) is associated with the intersection of the Azores archipelago and the Mid-Atlantic Ridge at 38–39°N (Azores Platform). In contrast to the low ^3He/^4He Jan Mayen plume, the Azores Platform anomaly has high ^3He/^4He associated with radiogenic ^{206}Pb/^{204}Pb and incompatible element enrichment (elevated (La/Sm)$_N$). In addition, two distinct short-wavelength anomalies occur at 1) 35°N, also referred to as the Great Meteor Anomaly [*Rideout and Schilling,* 1985] or the "north of Oceanographer fracture zone anomaly" [*Shirey et al.,* 1987]; and 2) 34°50′ [*Hekinian et al.,* 2000; *Niu et al.,* 2001; *Pineau et al.,* 2004; *Cartigny et al.,* 2008].

New data in this study include δD_{SMOW} (TC/EA) and δ^7Li (presented in S3.2 below). H_2O and Ce concentrations for Azores platform basalts were reported in *Dixon et al.* [2002]. These data are summarized in Figure S2-10, omitting data from highly vesicular basalts due to water

degassing (described below). Azores Platform basalts have lower H_2O/Ce than Arctic Ridge basalts, however both are higher than MORB from the southern Atlantic and Pacific (H_2O/Ce = 170 ± 15 [*Michael*, 1995].

Shallow Modification of Water: *Dixon et al.* [2002] evaluated degassing of water in Azores Platform basalts and found significant loss of water from basalts erupted on or near the shallow summit of the Azores platform (926 - 1,950 m). These samples (17-5, 19-1, 21-5, 22-5 & 6, 29-1) are highly vesicular (25 vol.% - 60 vol.%) and have lost about 10% to 30 % of their initial water into vesicles (Figure S2-11). Given the large uncertainties in the calculated bulk volatile values associated with bubble loss or accumulation, samples with >25 vol.% vesicles are excluded from subsequent figures showing variations in H_2O or H_2O/Ce, but included in figures showing δD_{SMOW}.

Similarly, highly vesicular (5-65 vol.% vesicles) samples erupted at the 35°N anomaly (44-1, 45, 46, and 9-10) and at 34°50′N (OT3-9, OT3-10 [*Pineau et al.*, 2004]) have vesicularity that correlates roughly inversely with depth (5 vol.% at 3,900 m to 60 vol.% at 1,657 m). Samples erupted shallower than 2500 m (9-10, 44-1, 45, 46, and RC136) are highly vesicular (>25 % vesicles). Both dissolved and bulk water concentrations at a given Ce for these vesicular samples are significantly lower than other Azores platform samples. *Dixon et al.* [2002] interpreted the low H_2O concentrations in the vesicular samples as an indication of a water-poor EM component. In the context of additional data (e.g., lack of correlation with Ba/Nb), we now prefer an interpretation that the low H_2O/Ce in the vesicular samples is caused by gas loss during shallow degassing.

During water degassing under equilibrium conditions, hydrogen isotopes fractionate, resulting in heavier vapor phase and lighter residual melt. The hydrogen isotopic fractionation between vapor and melt (δ_{v-m}) is between 40 ‰ and 32 ‰ for basalts containing 0.5 to 1 wt. % water [*Pineau et al.*, 1998; *De Hoog et al.*, 2009]. Isotopic fractionation decreases as the amount of dissolved water increases, related to changes in water speciation [*Stolper,* 1982]. *Kingsley et al.* [2002] show that water degassing is unable to produce the full range of observed δD_{SMOW} in the EMP-ESC samples, however it may have a measurable impact on the most vesicular samples along the Azores Platform and EMP-ESC. *Dixon et al.* [2002] estimate the percent of H_2O degassed from each sample. We can predict the change in the δD_{SMOW} assuming the conservative case of closed system equilibrium degassing: $\delta D_{melt} = \delta D_{initial} - 1000ln\alpha(F)$ [*Taylor and Sheppard*, 1986], where F = mass fraction of H_2O degassed and $1000ln\alpha \approx \delta D_{vesicle}$ (gas) - δD_{basalt} (melt) = δ_{v-m}. Expected isotopic shifts due to water degassing using δ_{v-m} of 30 ‰ to 40 ‰ are shown below (Table S2-2).

The primary magmatic δD_{SMOW} for highly vesicular basalts may be 2 ‰ to 13 ‰ heavier that the measured values. This is within the uncertainty in accuracy between the two analytical techniques used and does not impact the conclusions of this study, but does need to be taken into account for the discussion of hydrogen isotopic compositions of mixing end-members.

S2.5 Southern Atlantic

Sample Locations and Provenance: Fresh glassy MORB glasses from the URI collection of J.-G. Schilling were dredged along the Mid-Atlantic Ridge between 40°S and 54°S during the R. V. *Maurice Ewing* EW93-09 cruise (Figure S2-12).

Regional Geochemical Trends: This section of the ridge contains two distinct geochemical, gravitational, and bathymetric anomalies. The northern "Discovery" anomaly is centered at 47.5°S and is influenced by the Discovery plume [*Douglass et al.,* 1995 and 1999]. The Discovery Tablemount (42°S, 0°), formed by the Discovery plume volcanism 25 Ma years ago, is northeast of the present location of the Discovery plume [*Kempe and Schilling*, 1974; *Douglass et al.,* 1995 and 1999]. The southern "Shona" anomaly is centered at 51.5°S [*leRoex et al.,* 1987; *Douglass et al*., 1995 and 1999]. Discovery anomaly lavas show a wide range of $^{87}Sr/^{86}Sr$ at relatively constant $^{206}Pb/^{204}Pb$, consistent with mixing of PacDM and EM components [*Douglass and Schilling*, 2000; *Andres et al.,* 2002] (main text Figure 4a). Discovery basalts with high $^{87}Sr/^{86}Sr$ also have high Ba/Nb (main text Figure 4b). A few Discovery basalts have elevated $^{3}He/^{4}R_a$ up to 15 R/R_a, but there is no overall correlation with latitude, $^{206}Pb/^{204}Pb$, or Ba/Nb. Shona anomaly glasses form two Pb-Sr isotopic groups consistent with variable contributions of PREMA- and EM-type components. Shona Group I lava compositions show mixing mainly between PacDM and an enriched PREMA-type component similar to that for the Easter Salas Y Gomez plume (SYG*). Shona Group I lavas have uniform $^{3}He/^{4}He$ of ~8. Shona Group II lava compositions show additional influence of an EM component [*Andres et al.*, 2002]. Shona Group 2 lavas have elevated $^{3}He/^{4}He$ up to 12 R/R_a.

Shallow Modification: All South Atlantic glasses are erupted between 1720 and 3900 m water depth. Vesicularity and H_2O/Ce do not correlate with depth, suggesting that H_2O concentrations have not been modified by shallow degassing [*Dixon et al.,* 2002].

Samples 9, 19, and 23 have high H_2O, H_2O/Ce and δD_{SMOW} that are outliers on the overall geochemical trends (Figures S2-14 and 15). δD_{SMOW} for glass 19D-1, which has anomalously high H_2O concentration, has a δD_{SMOW} value similar to the other glasses, suggesting that the contaminant is not seawater ($\delta D_{SMOW} = 0$ ‰). *Dixon et al.* [2002] interpreted sample 19 as having assimilated serpentine during ascent. We suggest that samples 9 and 23, and to a lesser extent samples 22 and 26, have also assimilated a hydrous component (seawater/brine/serpentine) during ascent or residence in the crust. H_2O and H_2O/Ce in samples 19 and 23 will be excluded from further consideration. Sample 9 is included, but its water concentration may be higher than the primary magmatic value.

S2.6 Southern Pacific: Pacific Antarctic Ridges (PAR), Macquarie Ridge, Easter Microplate – Salas y Gomez Seamount Chain (EMP-ESC)

Sample Locations and Data Sources: New δD_{SMOW} data generated in this study are compared to published data from three southern Pacific regions: 1) Easter Microplate (EMP) and Easter Salas y Gomez Seamount Chain (ESC) [*Kingsley and Schilling,* 1998; *Cheng et al.,* 1999; *Kingsley et al.,* 2002]; 2) the Pacific-Antarctic Ridge 41° to 65°S (PAR) [*Vlastélic et al.,* 2000; *Hamelin et al.,* 2010 and 2011; *Clog et al.,* 2013]; and 3) Macquarie Island [*Kamenetsky et al.,* 2000; *Bindeman et al.* 2012]. Sample locations are shown in Figures S2-16 and S2-17.

Regional Geochemical Trends: The ESC-EMP is a 1400km long volcanic feature, along which regular gradients in Pb and Sr radiogenic isotope and trace element contents (Figure S2-18) reflect progressive dilution of the Salas y Gomez mantle plume with the depleted upper-mantle, as it flows along a sublithospheric channel toward the East Pacific Rise at the latitude of the Easter Microplate [*Fontignie and Schilling*, 1991; *Hanan and Schilling*, 1989; *Kingsley and*

Schilling, 1998; *Pan and Batiza*, 1998; *Schilling et al.*, 1985; *Cheng et al.*, 1999; *Kingsley et al.*, 1997; *Kingsley et al.,* 2002].]. Elevated ^{3}He/^{4}He up to ~12.5 occur along the ESC, but there are no systematic correlations with other indicators of mantle enrichment. The Salas y Gomez plume component was described as HIMU by *Kingsley et al.* [2002} and is described as PREMA in this study. Overlapping radiogenic isotopic compositions for these three regions (Figure S2-20) suggests influence by a common component with high ^{206}Pb/^{204}Pb similar to that for the Easter Salas y Gomez (SYG) plume, even for ridges far from hotspots.

H_2O correlates positively with Ce ranging from about 140 in the depleted EMP basalts to about 230 for the enriched ESC basalts (Figure S2-19) omitting samples that have degassed or assimilated brine as documented below [*Simons et al.,* 2002].

Shallow Modification: *Simons et al.* [2002] document both degassing loss of H_2O in the most fractionated and enriched ESC glasses, as well as gain of Cl and H_2O due to seawater or brine assimilation in the more depleted glasses. EMP samples 26-1, 30-1, 35-1, and 38-1 have anomalously elevated Ba/Nb, H_2O/Ce and δD_{SMOW}, but not ^{87}Sr/^{86}Sr, at a given ^{206}Pb/^{204}Pb relative to the overall trends (Figures S2-20 to 23) consistent with assimilation of seawater or hydrothermal brine. These samples are omitted from the plots in the main text, but shown here for completeness.

S2.7 Northern Pacific:
Sample Locations and Provenance: Northern EPR basalts from 6° to 17°N were sampled during CHEPR Expedition in 1985 [*Langmuir et al.*, 1986] and Raitt 02 Expedition in 1986 [*Batiza et al.*, 1990] along a 350-km-long segment of the fast-spreading (~10-12 cm/yr) EPR (Figure S2-24). Volatile and halogen data have been reported for melt inclusions in phenocrysts from the Siqueiros Fractures [*Saal et al.*, 2002] and for glasses from EPR in this region [*le Roux et al.*, 2006].

Regional Trends: This region of the EPR is unaffected by hotspots. Heterogeneities sampled by the basalts are dispersed within the upper mantle. *Castillo et al.* [2000] show a schematic illustration of the nature and distribution of dispersed small-scale heterogeneities in the mantle source for EPR basalts with PREMA-type (their seamount-type) heterogeneities dominating from 11° to 14°N and EM-type (their Indian MORB-like) dominating north of 14°N, but both types of heterogeneities are present in lesser amounts in both regions (Figure S2-25).

H_2O concentrations determined by TC/EA range from 0.06 to 0.4 wt. % (Figure S2-26), in good agreement with water concentrations determined on other basalts from this area [e.g., *Michael,* 1995; *Danyushevsky et al.*, 2000; *le Roux et al.,* 2006].

Shallow Modification. These samples are not believed to have undergone significant shallow-level modification.
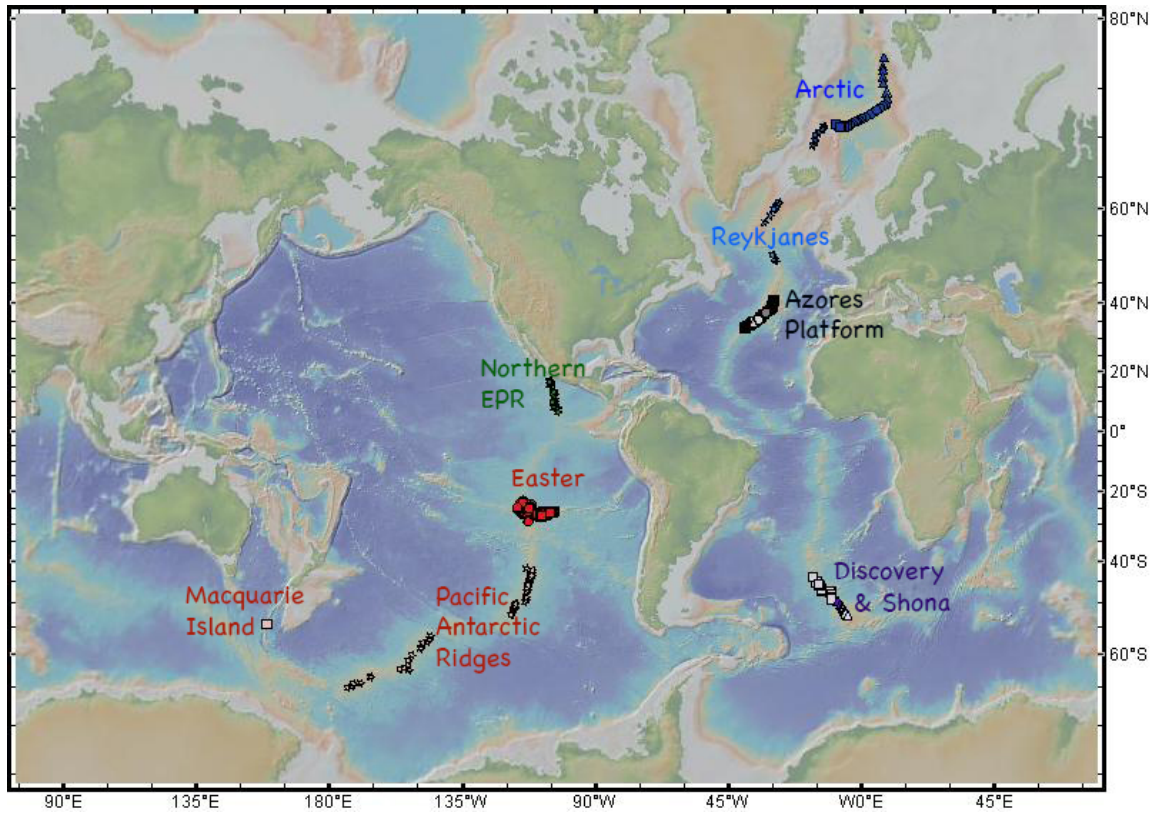
Figure S2-1. Sample locations for samples discussed in this paper. Base map courtesy of Geomapapp - http://www.geomapapp.org/.
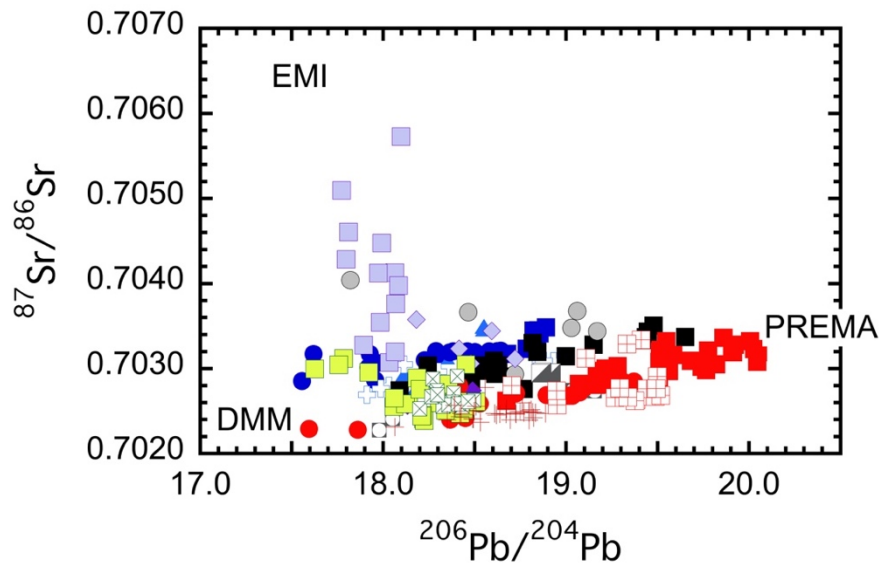
Figure S2-2. Published radiogenic isotopic compositions of samples used in this study. EM-type basalts have high $^{87}Sr/^{86}Sr$ and low $^{206}Pb/^{204}Pb$. PREMA-type basalts have low $^{87}Sr/^{86}Sr$ and high $^{206}Pb/^{204}Pb$. Basalts from EMP-ESC, Macquarie Island, south Pacific, and Azores Platform form DMM-PREMA mixing arrays. Azores Platform DMM-PREMA array is shifted toward higher $^{87}Sr/^{86}Sr$ (EM) values than EMP-ESC. Basalts from the southern MAR Discovery anomaly form a DMM-EM array. Arctic Ridge basalts form an EM-PREMA array, most clearly displayed by Mohns Ridge basalts. Some basalts from the Reykjanes also shows EM-PREMA array, but shifted to lower $^{87}Sr/^{86}Sr$ values than the Arctic Ridges. Symbols are used consistently throughout paper. Radiogenic isotopic data from: Arctic Ridges [*Schilling et al.,* 1999]; Reykjanes Ridge [*Kelley et al.* 2013]; Azores Platform FAZAR [*Dosso et al.,* 1999; *Gale et al.,* 2013]; MAR 34°N [no data] and 14°N [*Dosso et al.,* 1991]; EMP-ESC [*Kingsley and Schilling*, 1998; *Cheng et al.,* 1999]; southern MAR 40° to 54°S Shona and Discovery anomalies [*Douglass et al.,* 1999]; southern Pacific Ridges (41° to 65°S) [*Vlastélic et al.,* 2000; *Hamelin et al.,* 2010 and 2011]; Macquarie Island [*Kamenetsky et al.,* 2000]; EPR 6° to 17°N [*Castillo et al.,* 2000; *Gale et al.,* 2013]; EPR 12°50'N [*Hekinian et al.,* 1989].
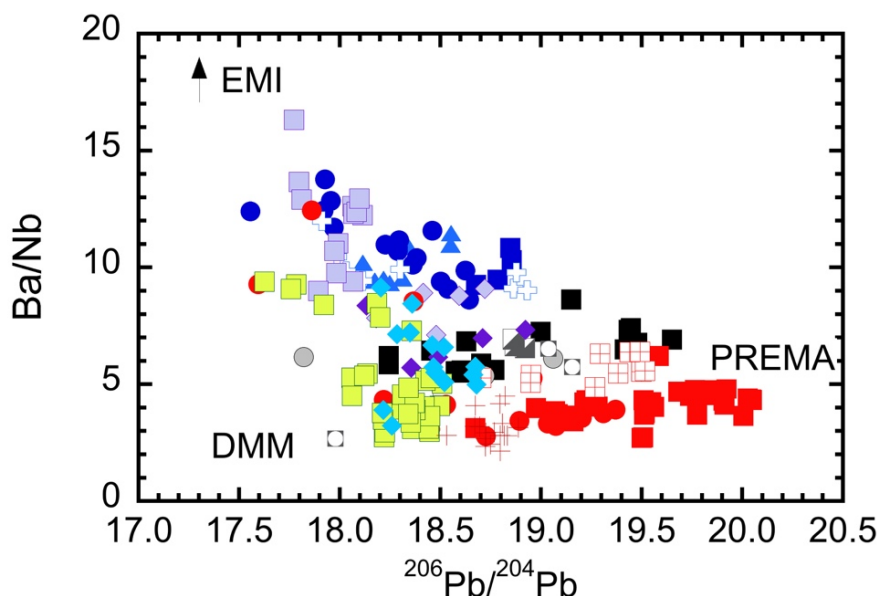
Figure S2-3. Published Ba/Nb versus $^{206}Pb/^{204}Pb$ compositions of basalts used in this study. EM-type basalts have low $^{206}Pb/^{204}Pb$ and high Ba/Nb. PREMA-type basalts have high $^{206}Pb/^{204}Pb$ and low Ba/Nb. Most Easter, Macquarie, Shona Group 1, and Azores Platform samples are described by mixing between DMM and PREMA end-members with small amounts of EM. Southern Pacific basalts are consistent with average EPR composition, not the DMM end-member. Macquarie basalts are enriched with PREMA + small EM component, and are not representative of depleted or even average MORB. Azores Platform DMM-PREMA array are shifted toward higher $^{87}Sr/^{86}Sr$ (EM) values compared to EMP-ESC array. Discovery samples lie on the DMM-EM array, with EM basalts enriched in incompatible elements. Arctic Ridge samples lie on the EM-PREMA array, shown by Mohns Ridge basalts. In this case the DMM-EM end-member is strongly depleted in incompatible elements. Reykjanes samples also lie on EM-PREMA array similar to Mohns, but shifted to lower $^{87}Sr/^{86}Sr$ and Ba/Nb values. Some Easter Microplate and EPR (10° to 17°N) basalts have high Ba/Nb and fall off the DMM-PREMA array consistent with mixing with EM component. Trace element data for Arctic Ridges [*Trønnes et al., 1999; Kelley et al., 2013*]; Reykjanes Ridge [*Kelley et al.* 2013]; Azores Platform FAZAR [*Gale et al.,* 2013]; MAR 34°N [*Niu et al.,* 2001] and 14°N [*Bougault et al.,* 1988; *Dosso et al.,* 1993]; EMP-ESC [*Kingsley and Schilling*, 1998; *Kelley et al., 2013*]; southern MAR 40° to 54°S Shona and Discovery anomalies [*Douglass et al.,* 1995; *Kelley et al.,* 2013]; southern Pacifc Ridges (41° to 65°S) [*Vlastélic et al.,* 2000]; Macquarie Island [*Kamenetsky et al.,* 2000]; EPR 6° to 17°N [*Castillo et al.,* 2000; *Gale et al.,* 2013]; EPR 12°50'N [*Hekinian et al.,* 1989].
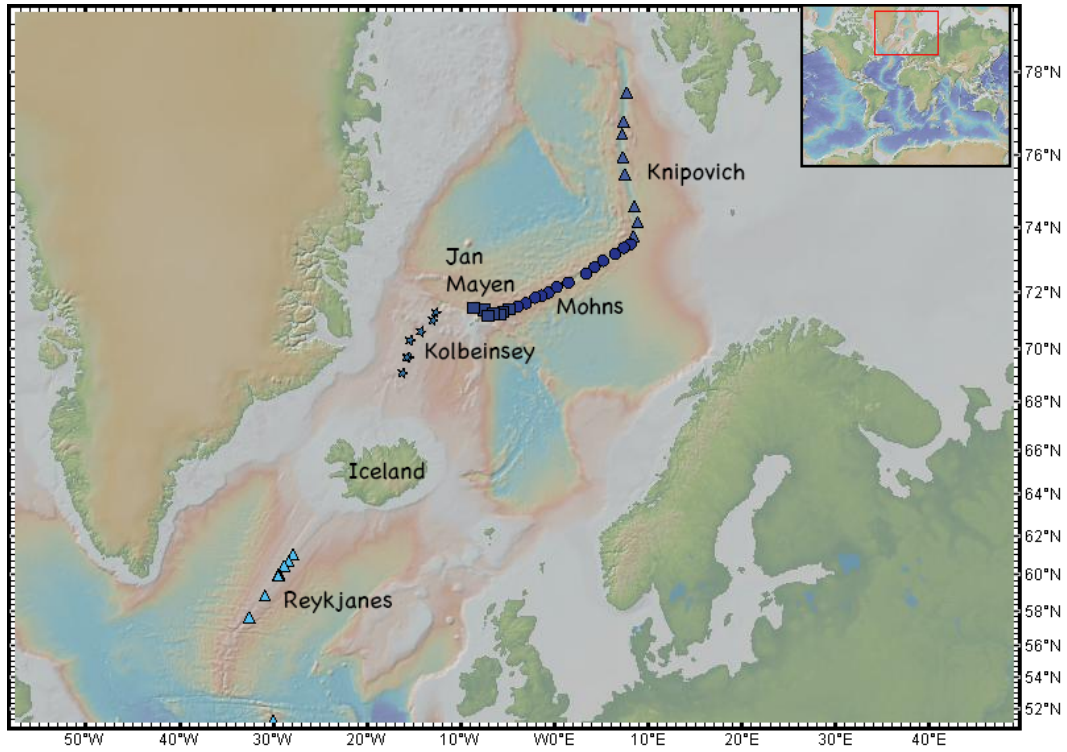
Figure S2-4. Locations of Arctic and Reykjanes Ridge basalts. Base map courtesy of Geomapapp - http://www.geomapapp.org.
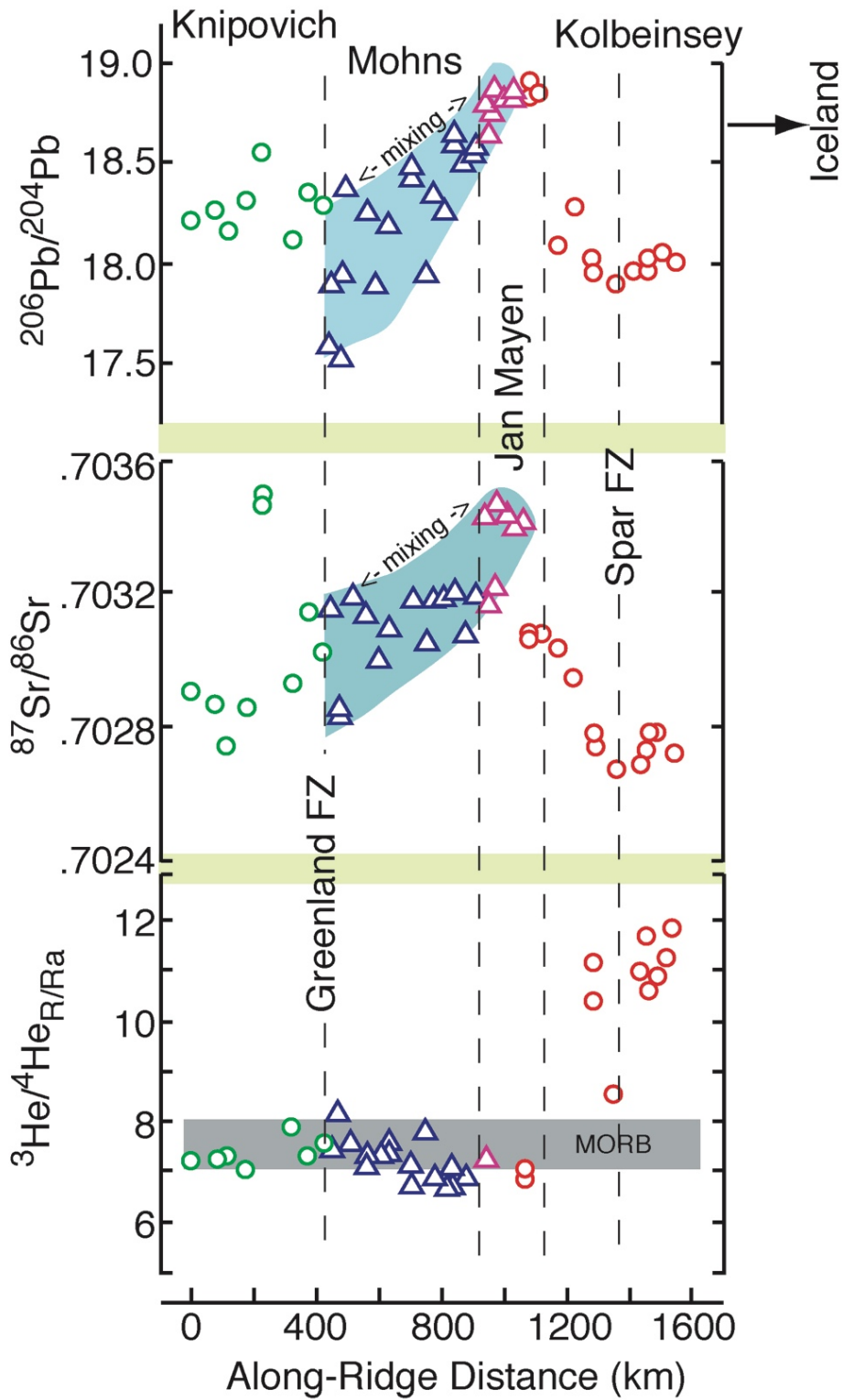
Figure S2-5. Regional geochemical trends in Arctic Ridge basalts. Symbols differ from those used in the main text.
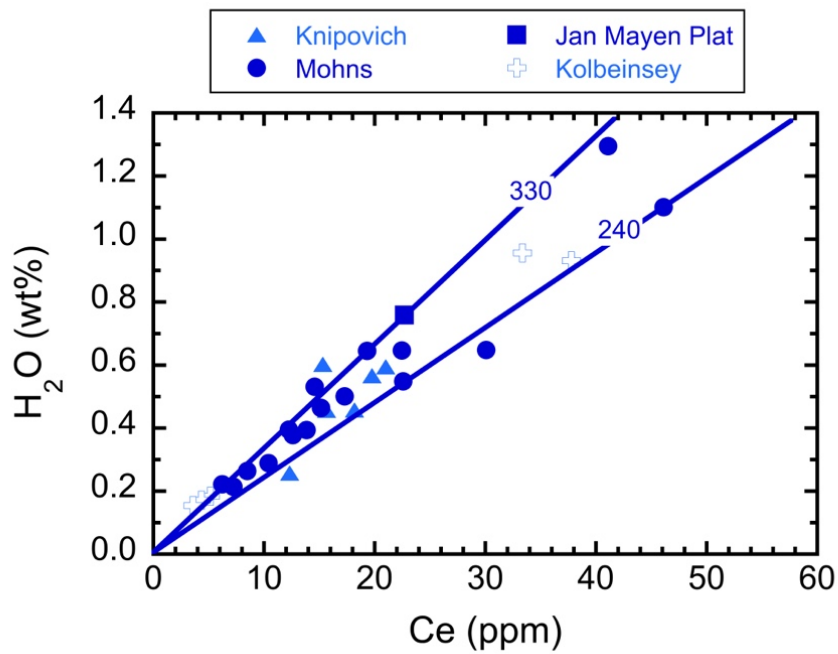
Figure S2-6. Positive correlation between H_2O and Ce for Arctic Ridges. Mean H_2O/Ce ~310 ± 60 greater than typical MORB from south Atlantic and Pacific (~170 ± 15) [*Michael*, 1995].
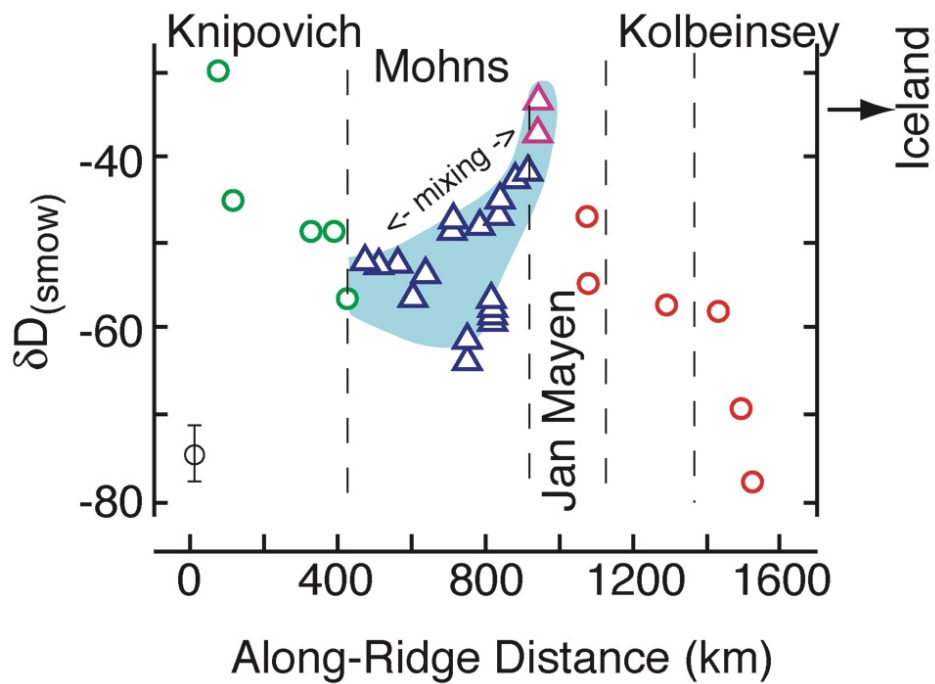
Figure S2-7. Hydrogen isotope ratios as a function of distance along the Arctic MAR from 80°N. Data from this study and *Poreda et al.* [1986].
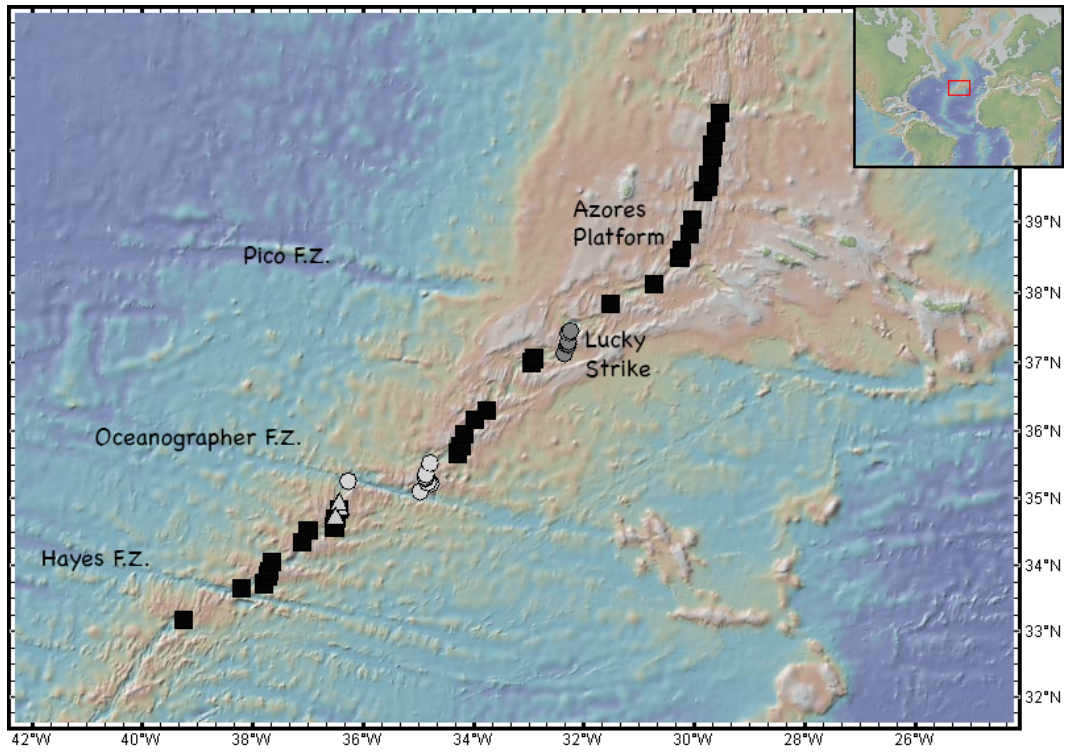
Figure S2-8. Locations of Azores Platform basalt samples [base map courtesy of Geomapapp - http://www.geomapapp.org/].
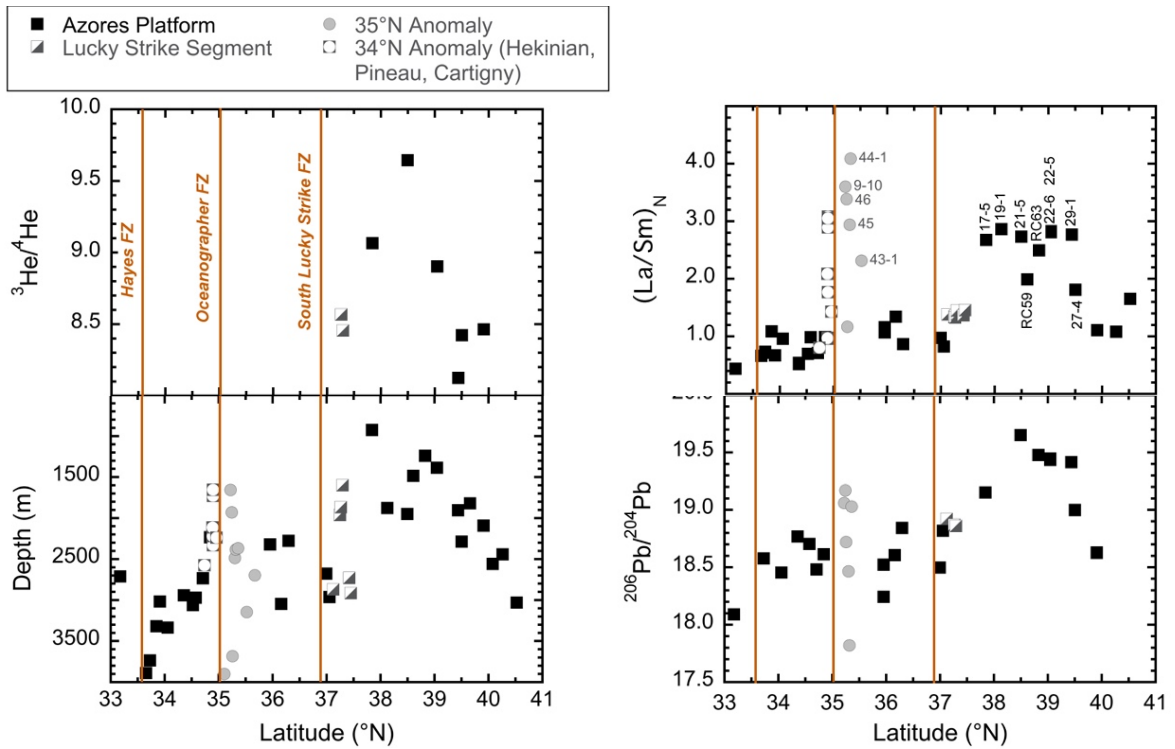
Figure S2-9. Variation in depth and selected geochemical parameters as a function of latitude.
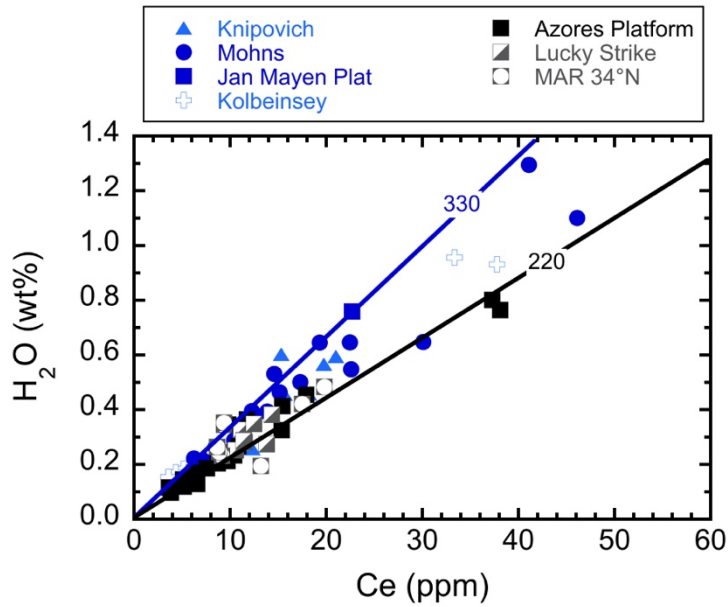
Figure S2-10. Correlation between H_2O and Ce in Azores Platform and Arctic Ridge basalts. Ce data sources given in caption to Figure S2-3. H_2O data from: Arctic Ridges (this study, FTIR); Reykjanes Ridge [*Poreda et al.,* 1986]; Azores Platform, Lucky Strike, and 35°N [*Dixon et al.,* 2002]; 34°50'N [*Pineau et al.,* 2004]. Note similarity to Figure S2-6.amd differences with other regions (below).
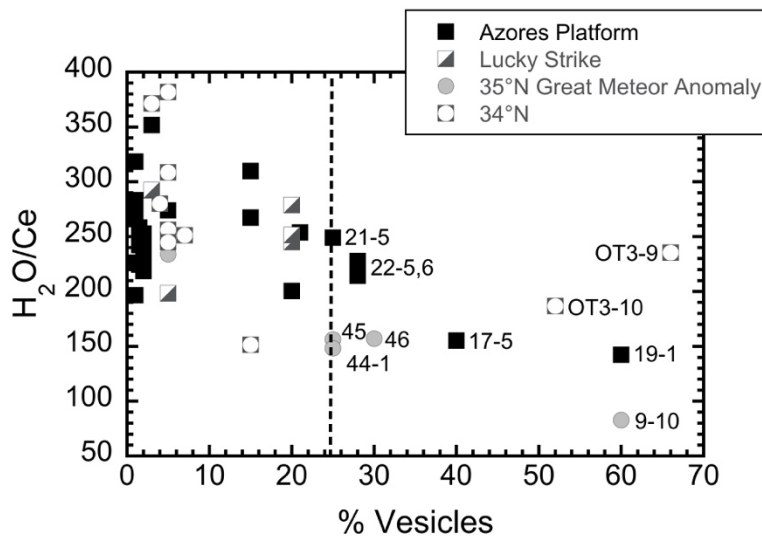
Figure S2-11. H_2O/Ce as a function of vesicularity, showing that water loss during degassing is significant for enriched samples erupted at shallow depths.
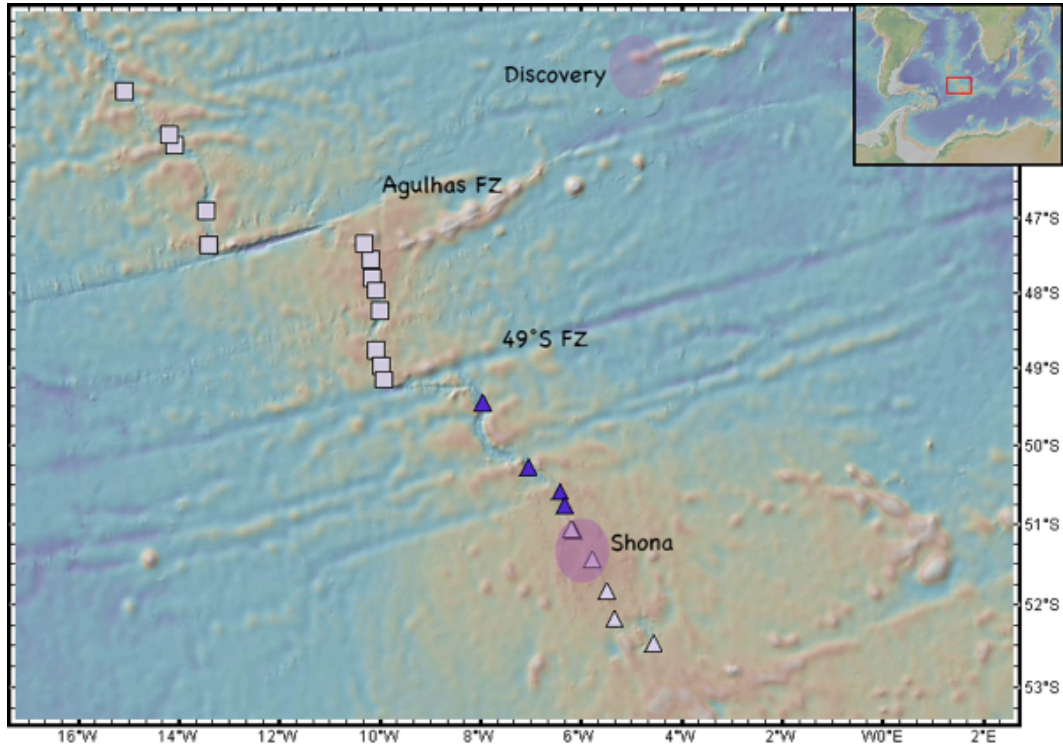
Figure S2-12. Location of southern Atlantic basalt samples. Base map courtesy of Geomapapp - http://www.geomapapp.org/.
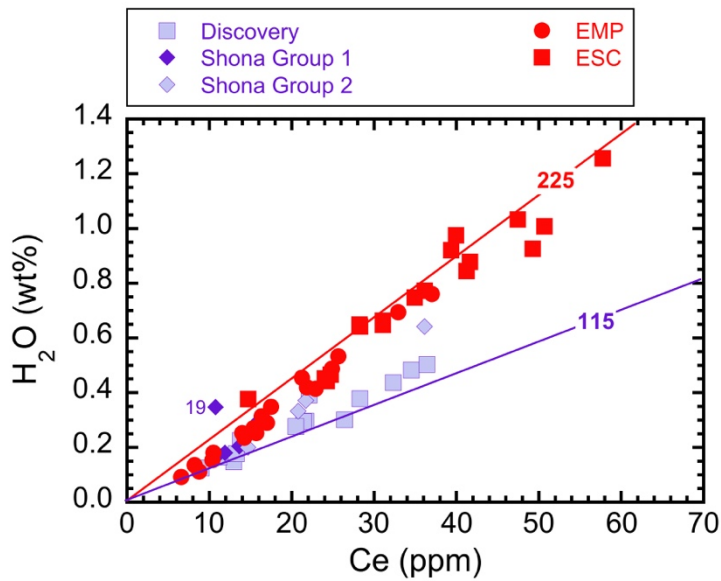
Figure S2-13. H_2O data for southern Atlantic [*Dixon et al.,* 2002] and EMP-ESC basalts [*Simons et al.,* 2002] omitting samples that have undergone shallow modification (see S2-14). H_2O correlates positively with Ce in each region. Discovery basalts have lower mean H_2O/Ce (136 ± 10) than EMP-ESC basalts.
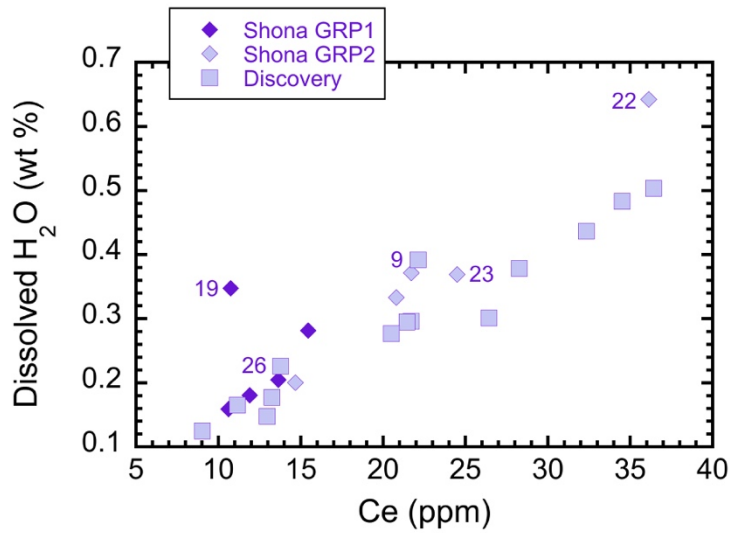
Figure S2-14. Southern Atlantic basalts 9, 19, and 22, and to a lesser extent samples 23 and 26, have water concentrations in excess of that expected based on the expected positive correlation between H_2O and Ce.
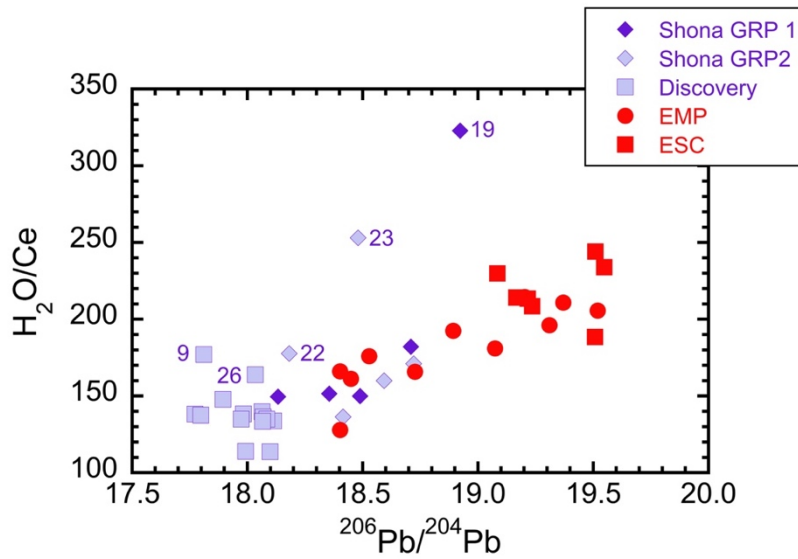
Figure S2-15. Southern Atlantic basalts 9, 19, and 23, and to a lesser extent samples 22 and 26, have water concentrations in excess of that expected from the overall correlation between H_2O and $^{206}Pb/^{204}Pb$ observed for each region.
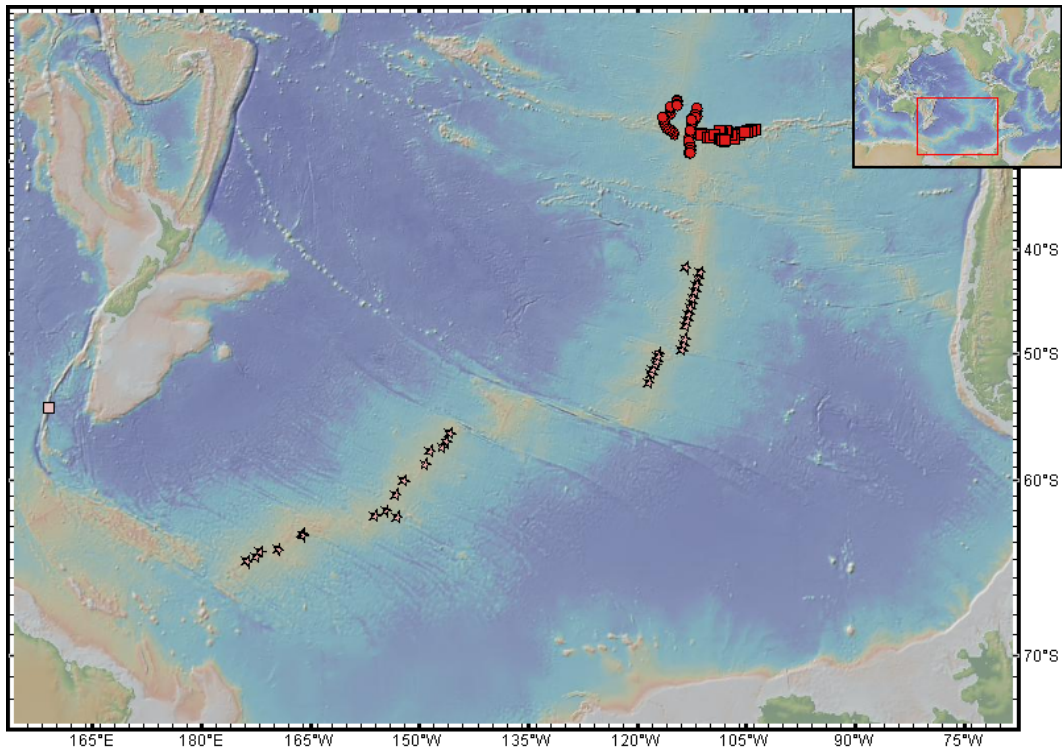
Figure S2-16. Location of EMP-ESC, PAR, and Macquarie Island basalt samples (see references in text). Base map courtesy of Geomapapp - http://www.geomapapp.org/.
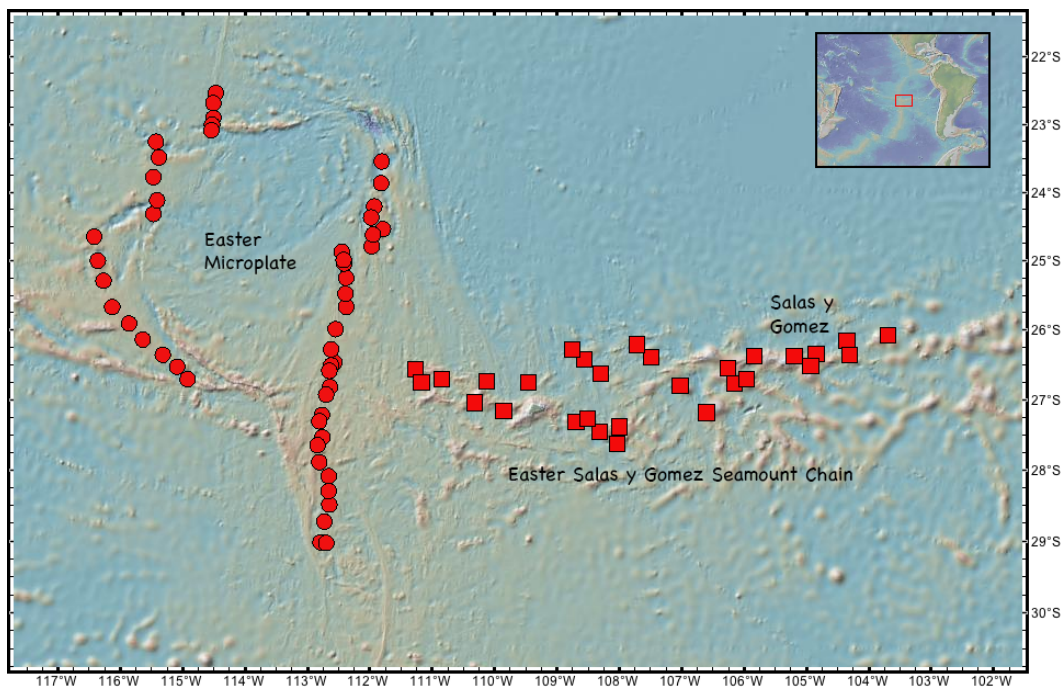
Figure S2-17. Location of EMP-ESC basalt samples (see references in text). Base map courtesy of Geomapapp - http://www.geomapapp.org/.
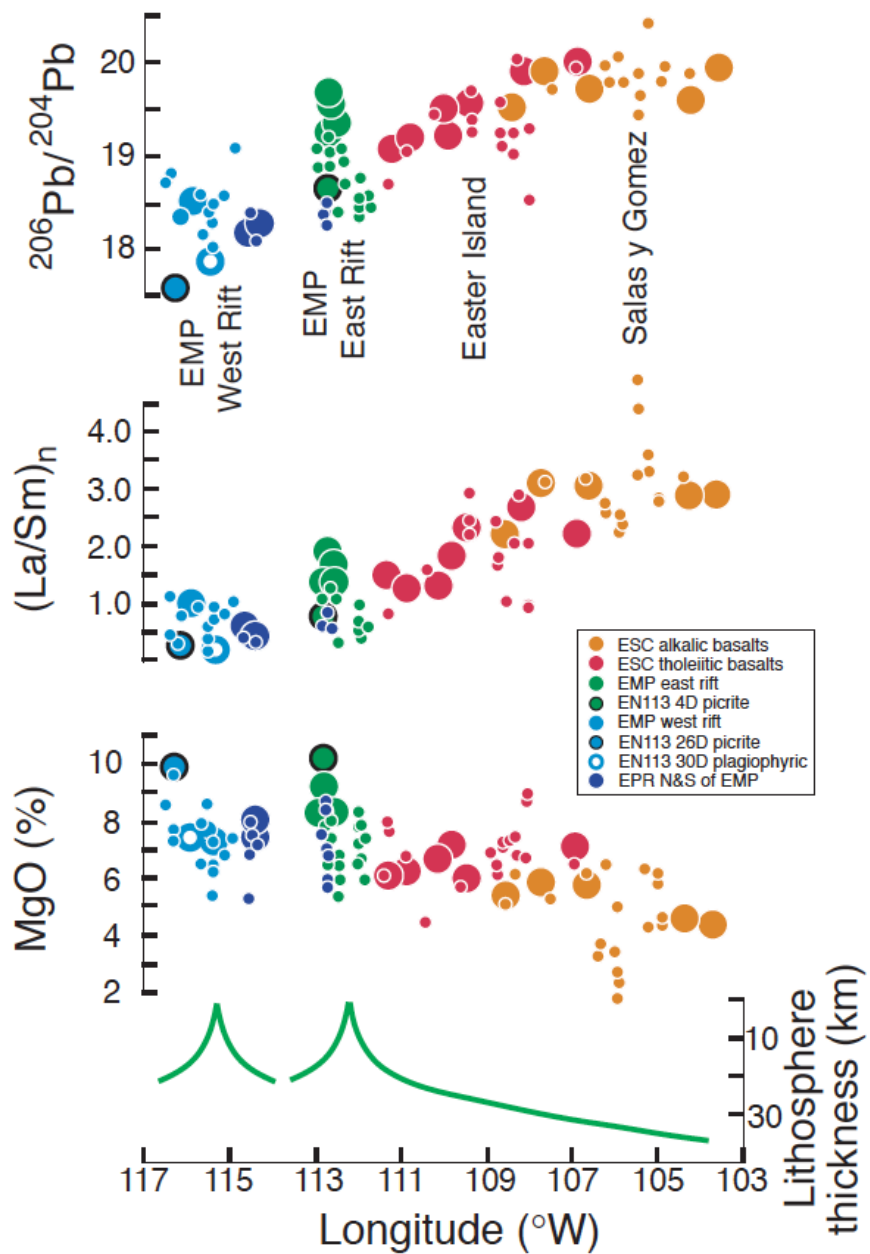
Figure S2-18. Geochemical gradients in $^{206}Pb/^{204}Pb$, La/Sm$_N$ (normalized to chondrites), MgO content, and computed lithospheric thickness along the ESC and EMP as a function of longitude, taken from *Kingsley et al.* [2002] (their Figure 2a). Pb isotope data is from *Kingsley and Schilling* [1998], (La/Sm)$_N$ from *Kingsley et al.* [2002], and MgO data from *Pan and Batiza* [1998].
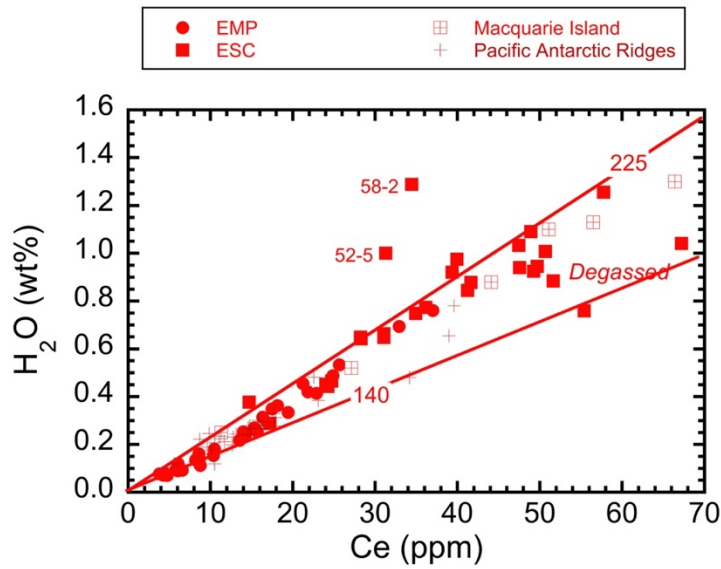
Figure S2-19. Positive correlation between H_2O and Ce for southern Pacific basalts.
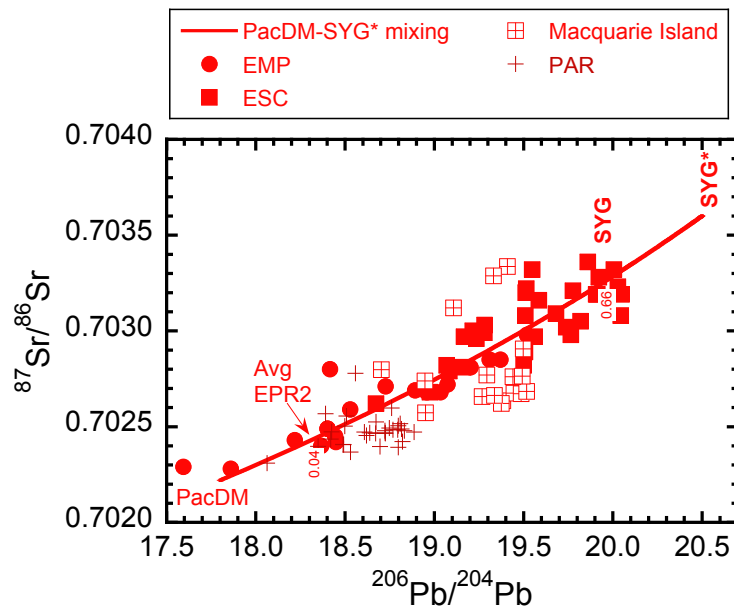
Figure S2-20. EMP samples 26-1, 30-1, 35-1, and 38-1(see next figure) have $^{87}Sr/^{86}Sr$ consistent with overall trend. Binary mixing model (curve) discussed in section S4.
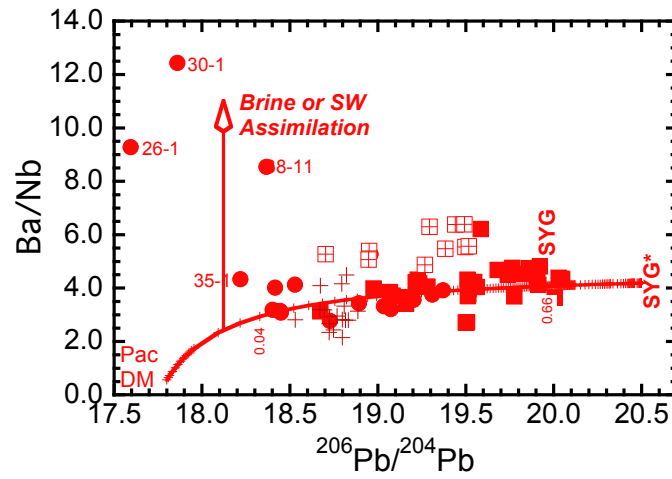
Figure S2-21. EMP samples 26-1, 30-1, 35-1, and 38-1 have anomalously high Ba/Nb relative to with overall trend, but are not anomalous in terms of strontium isotopes (Figure S2-20). "SW" is seawater. Binary mixing model (curve) is discussed in section S4.
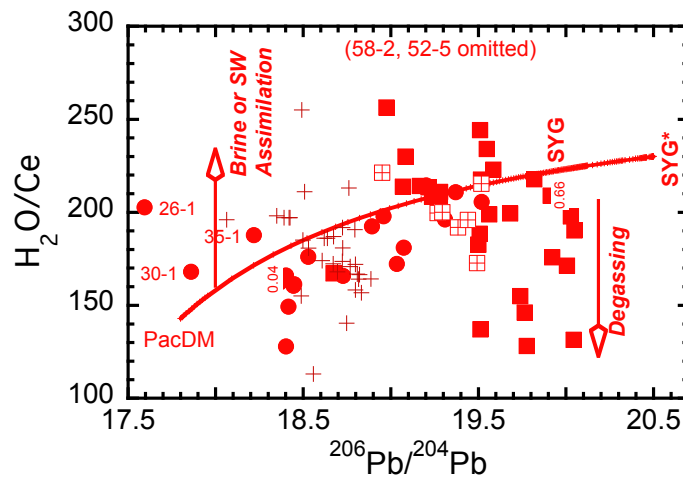
Figure S2-22. EMP samples 26-1, 30-1, 35-1, and 38-1 anomalously high H_2O/Ce relative to overall trend. "SW" is seawater. Binary mixing model (curve) is discussed in section S4.
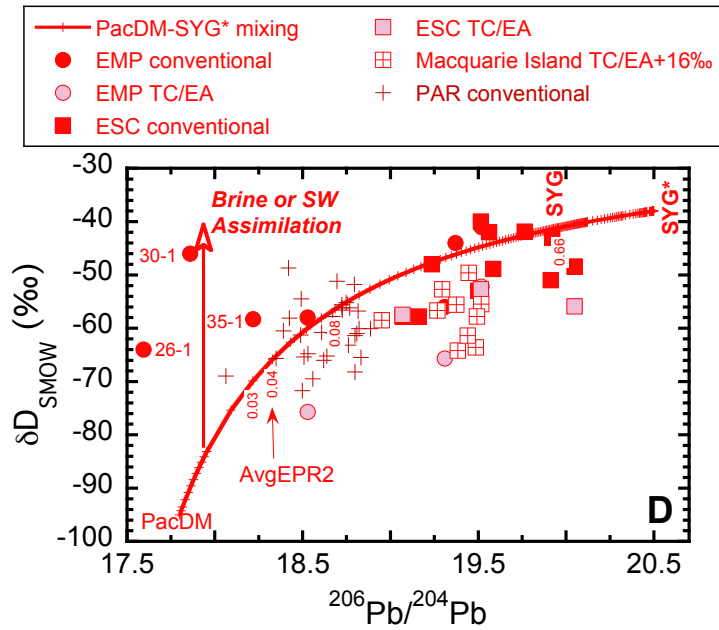
Figure S2-23. EMP samples 26-1, 30-1, 35-1, and 38-1 anomalously high δD_{SMOW} relative to overall trend. "SW" is seawater. Binary mixing model (curve) discussed in section S4.
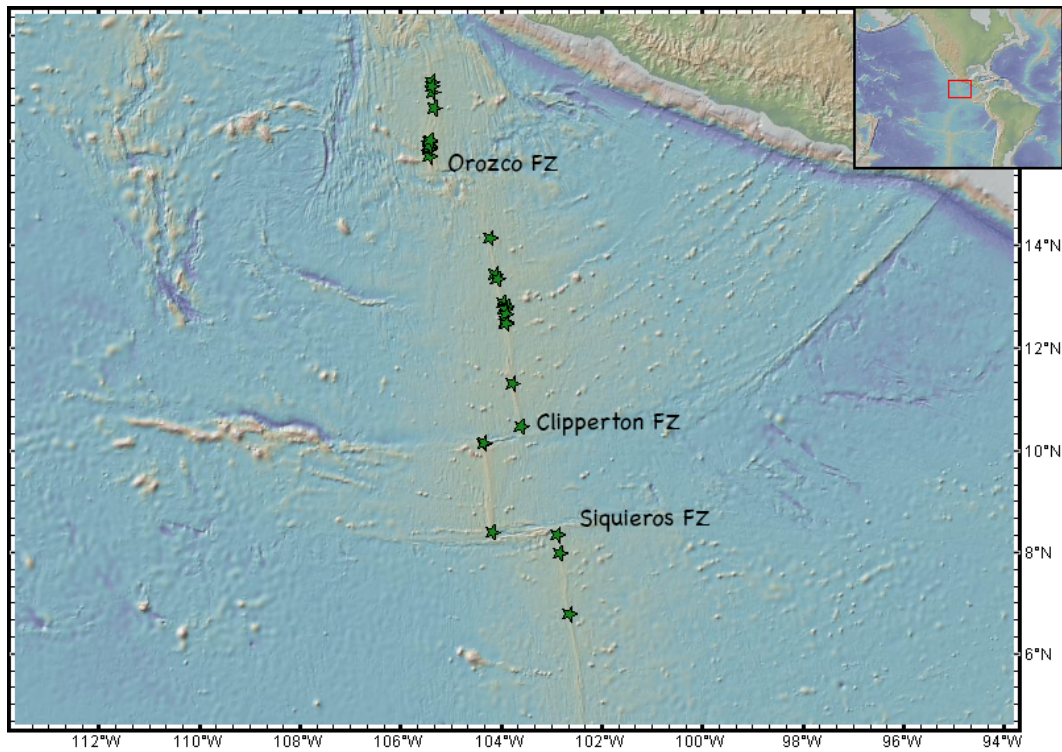
S2-24. Sample locations for northern EPR basalt samples Base map courtesy of Geomapapp - http://www.geomapapp.org/.
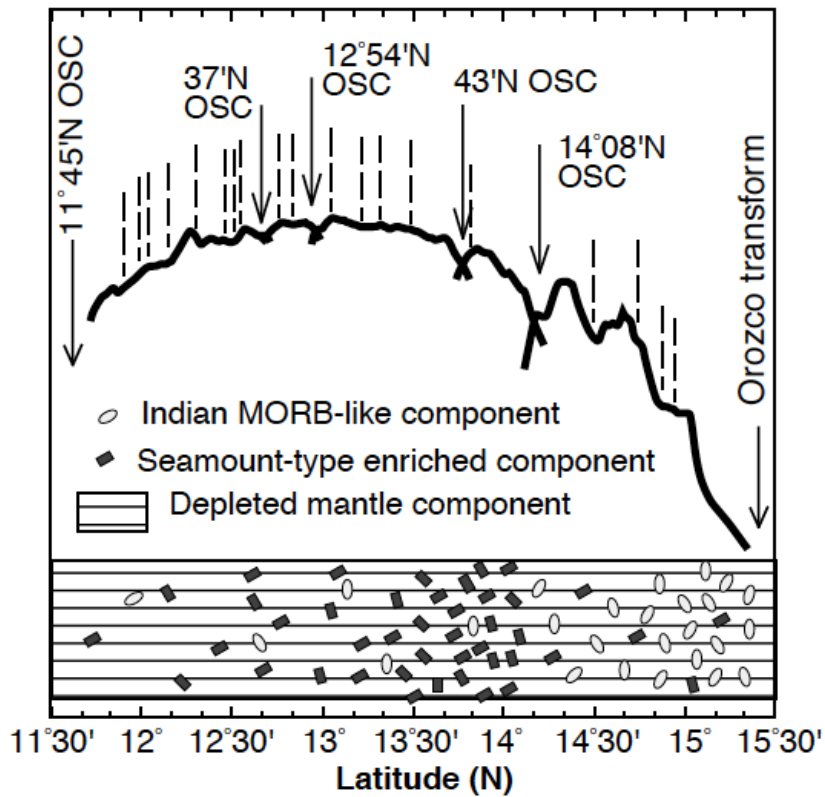
S2-25. Fig.17 [*Castillo et al.*, 2000] showing their model of dispersed heterogeneities. Using the nomenclature in our study, basalts north of ~15°N sample mostly EM-type heterogeneities, whereas basalts south of ~15°N sample mostly PREMA-type heterogeneities.
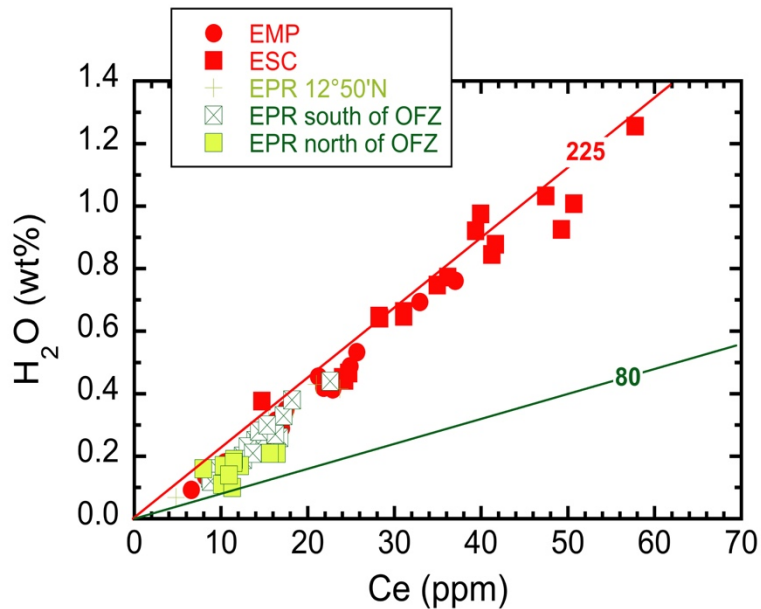
S2-26. H_2O versus Ce. H_2O in EPR basalts from this study (TC/EA). H_2O concentrations by TC/EA similar to those determined using FTIR for EMP. H_2O correlates positively with Ce for each region. In contrast to northern and southern Atlantic basalts, H_2O/Ce is as low as 80 in basalts north of Orozco FZ.

Azores Platform samples with >25% vesicles	Percent H_2O degassed [*Dixon et al.,* 2002]	‰ change in residual melt δD_{SMOW} ($\Delta_{v\text{-}m}$ = 30)	‰ change in residual melt δD_{SMOW} ($\Delta_{v\text{-}m}$ = 40)
17-5	12.4	-4	-5
19-1	31.4	-9	-13
21-5	20.1	-6	-8
22-5	16.5	-5	-7
22-6	18.5	-6	-8
(35°N) 44-1	16.3	-5	-7
(35°N) 45	5.2	-2	-2
(35°N) 46	8.5	-3	-4
(35°N) 9-10	32.6	-10	-13
(35°N) RC136	10.4	-3	-4

Table S2-1. Isotopic shifts due to water degassing.

S3. OTHER LIGHT STABLE ISOTOPE DATA

This section presents new δ^{18}O, δ^{7}Li and δ^{11}B data for the Arctic, Azores Platform, and Southern Atlantic samples, respectively. These data were not collected in all of our study regions and are not used in the modeling calculations. However, they provide additional checks on model results. We verified that in all cases, these light isotope data are consistent with model results, as described below.

S3.1 δ^{18}O in Arctic Ridge basalts

δ^{18}O values exhibit a very narrow range of 5.39 to 5.60 ‰ across the three ridge segments. Values for all these samples fall within the range (5.37 ‰ to 5.81 ‰) found by *Eiler* [2001] and *Cooper et al.* [2004] in studies of N-MORB glasses from the Mid Atlantic Ridge, East Pacific Rise and the Indian Ocean ridges (Figure S3-1). No clear trends of oxygen isotope ratios are evident with proximity to the Jan Mayen hotspot, radiogenic isotope ratios, trace element ratios, or major element variations in this region. The absence of correlations between oxygen isotopes and indicators of mantle enrichment suggests the volume of enriched components is small (<5%). This result is important because it supports a metasomatic model to produce mantle sources highly enriched in incompatible elements without addition of large quantities (5-25 %) of subducted sediments or altered igneous crust.

S3.2 δ^{7}Li in Azores Platform basalts

Lithium isotopic values in Azores Platform basalts vary from +3.2 to +5.7 ‰ and correlate positively with ^{206}Pb/^{204}Pb (Figure S3-2). These values are consistent with recently published δ^{7}Li data of 3.9 to 4.7 ‰ for Jan Mayen basalts [*Magna et al.,* 2011]. The heavier δ^{7}Li values for the PREMA end-member are consistent with previous results [*Nishio et al.*, 2005; *Elliott et al.,* 2006; *Krienitz et al.*, 2012], who showed that HIMU (PREMA)-type lavas are characterized by δ^{7}Li values up to +4.8‰, which they interpreted as being due to recycling of altered and dehydrated oceanic crust. Figure S3-3 shows the data and a binary mixing curve between our North Atlantic Depleted Mantle (NADM) and the Azores Platform C-O-H-CL fluid (AZ2*) with δ^{7}Li values of 3.0 and 5.1, respectively. Implications of the mixing models are discussed in the main text.

S3.3 δ^{11}B in Southern Atlantic basalts

Southern Atlantic depleted MORB samples (sample numbers 11, 14, 15, 18, 23, 26, 28, 41) have δ^{11}B values of about -9.5 ± 2 ‰ (Figure S3-4), lower than that normally cited for MORB (-4.0 ± 3.2 ‰), but similar to values reported for some OIB and primitive mantle [*Chaussidon and Jambon*, 1994; *Chaussidon and Marty*, 1995; *Gurenko and Chaussidon,* 1997; *Roy-Barman et al.,* 1998; *Tanaka and Nakamura*, 2005; *Turner et al.,* 2007; *Li et al.,* 2016]. The EM-type Discovery basalts have relatively constant δ^{11}B values of ~-7.2 ± 1.0 ‰ (Figure S3-4, 5, and 6). These values are within the range reported for OIB and are also consistent with the boron isotopic composition of dehydrated sediments (-1 to -8 ‰) [*Ishikawa and Nakamura*, 1993] and with dehydrated eclogite [*Zack et al.,* 2003]. Shona Group 1 samples 14, 15, 17 and 19 and Shona Group 2 sample 21 show a positive correlation between δ^{11}B and ^{206}Pb/^{204}Pb with values ranging from -9.8 to -3.8 ‰. Radiogenic isotopic and trace element ratios of these samples fall near the EMP-ESC array (Figure S2-4, 5, and 6) suggesting influence of a PREMA-type

component. The positive correlation between radiogenic and boron isotopic compositions suggests a heavy δ^{11}B PREMA end-member. Serpentine or serpentine-derived fluids may provide a source of heavy δ^{11}B with values of +8 to +13.0 ‰ [*Spivack and Edmond,* 1987; *Benton et al.,* 2001]. One complication to this interpretation is that Shona sample 19D-1 has the heaviest δ^{11}B (-3.8 ± 0.9 ‰) and also has anomalously high H_2O. The elevated H_2O has been interpreted as the result of assimilation of a hydrous component during ascent or residence in the crust. It is difficult to resolve the relative influence of deep versus shallow processes on the δ^{11}B in this sample with the available data.
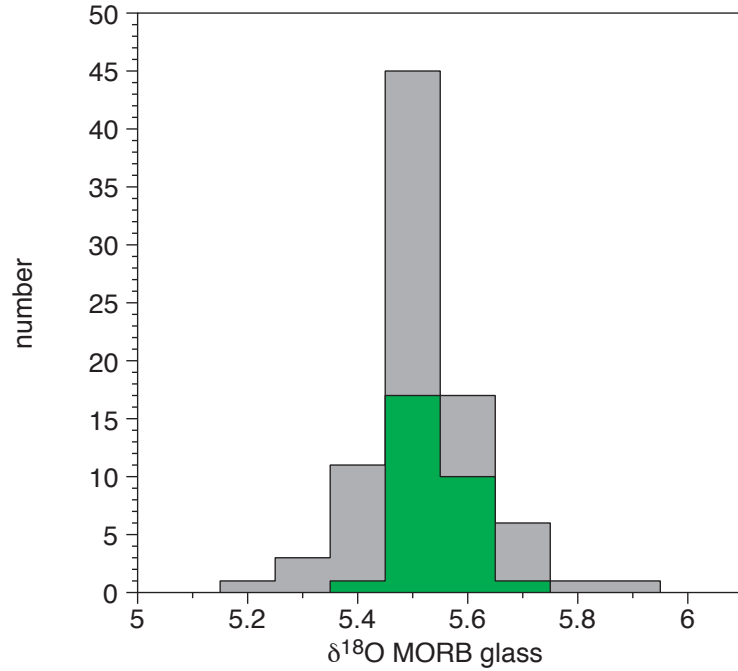
Figure S3-1. $\delta^{18}O$ values for Arctic Ridge basalts (green boxes, this study) are similar to those for global MORB (grey boxes, *Eiler* [2001]).
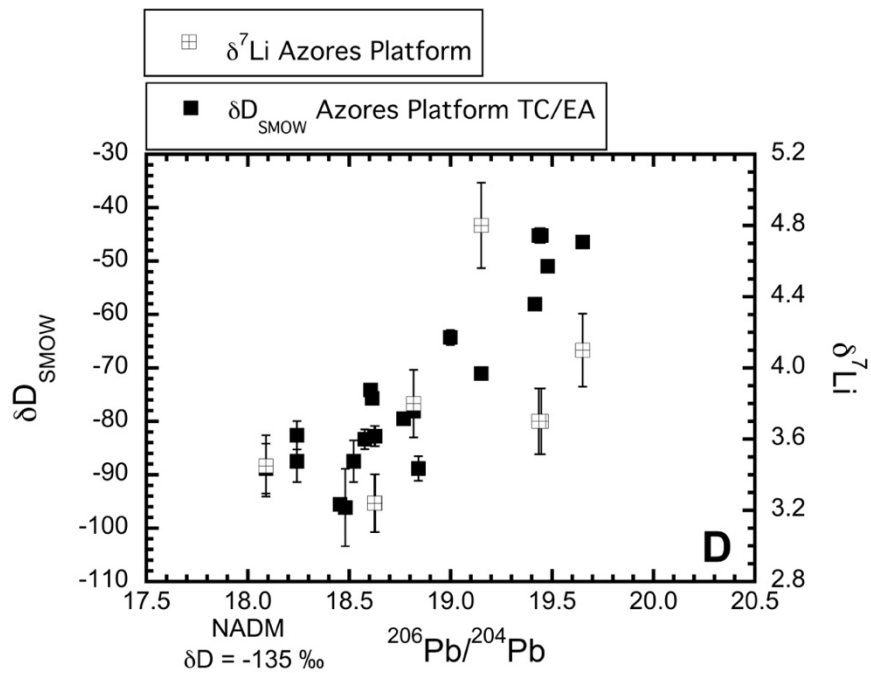
Figure S3-2. δ^7Li plotted with δD_{SMOW} versus $^{206}Pb/^{204}Pb$ showing that both correlate positively with $^{206}Pb/^{204}Pb$, consistent with heavier δ^7Li and δD_{SMOW} compositions in the PREMA end-member.
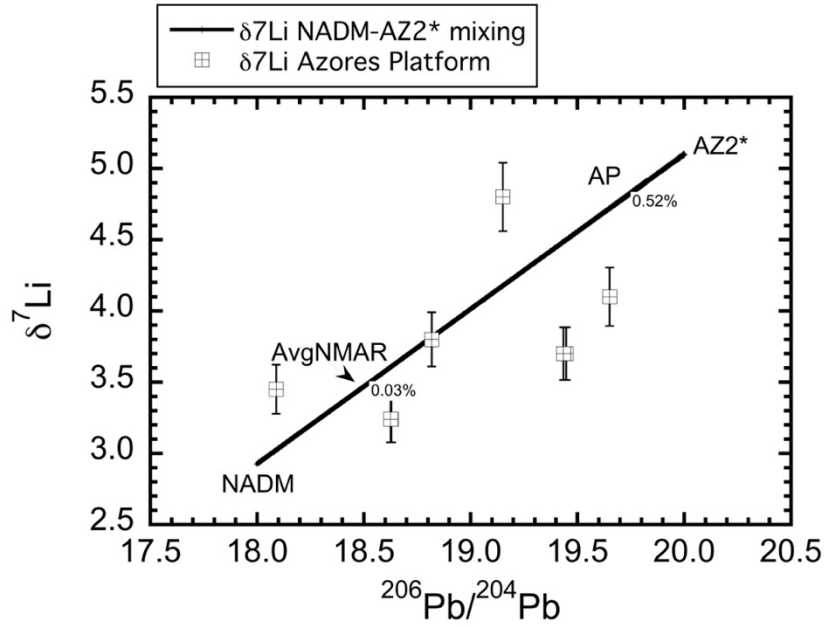
Figure S3-3. Mantle end-members for binary mixing curve listed (Table S4-1).
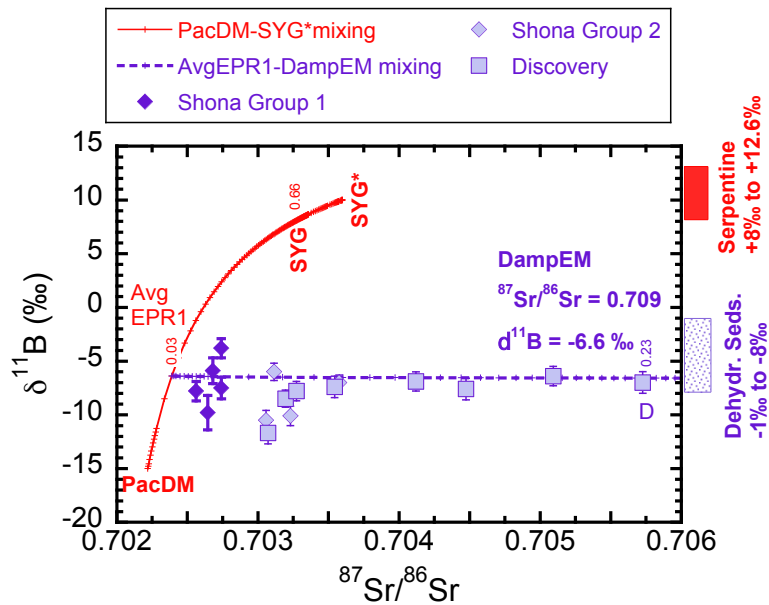
Figure S3-4. $\delta^{11}B$ versus $^{87}Sr/^{86}Sr$ in southern Atlantic basalts compared to binary mixing models (section S4).

S4. MIXING MODELS AND MANTLE END-MEMBER COMPOSITIONS

S4.1 Concentrations of Trace Elements in Mantle Sources

Determination of mantle source compositions for enriched MORB and OIB is notoriously difficult because estimates of absolute trace element concentrations depend on assumptions regarding extents of partial melting, source modal mineralogy, mineral-melt partition coefficients, and crystal fractionation corrections back to primitive magma [e.g., *Simons et al.,* 2002; *Asimow et al.,* 2004; *Workman et al.,* 2004; *Willbold and Stracke*, 2006; *Dixon et al.,* 2008]. Below we explore the feasibility of explaining the compositions of enriched MORB and OIB by addition of small amounts of incipient melts of subduction-modified sediments and igneous crust to depleted mantle. Our goal is to place self-consistent constraints on the proportions of mixing components using nonvolatile incompatible elements and to use these proportions to estimate the mantle end-member volatile and stable isotopic compositions. Binary mixing proportions are determined using an iterative forward model and minimum misfit criteria primarily based on radiogenic isotopes and ratios of similarly incompatible elements. Estimates of mantle end-member compositions are listed in Table S4-1. Mixing curves are calculated using standard binary mixing equations for elements (eqn. S4.1) and ratios (eqn. S4.2):

$$c_M = f_A c_A + f_B c_B = f_A c_A + (1 - f_A)c_B \qquad \text{(eqn. S4.1)}$$

$$R_M = \frac{1}{c_M}\left(\frac{(c_A c_B)(R_B - R_A)}{(c_A - c_B)}\right) + \frac{(R_A c_A - R_B c_B)}{(c_A - c_B)} \qquad \text{(eqn. S4.2)}$$

where c_X is the concentration of component X or in the mixture M and R_X is the isotopic ratio for component X.

S4.2 Models for North Atlantic PREMA and EM mantle end-members

S4.2.1 Azores Platform PREMA-type mantle component: *Asimow et al.* [2004] presented a comprehensive model for the major and trace element compositions of Azores Platform basalts. Mantle and melt compositions were estimated using a polybaric hydrous melting and fractionation model, which included 1) the role of H_2O on source on melting behavior (pHMELTS); 2) calculation of incremental primary liquid compositions following *Asimow et al.* [2001]; 3) calculation of aggregate melts using a mixing model that simulates a passive flow at depth and a transition to buoyantly driven active flow at 0.6 GPa; and 4) calculation of the role of H_2O in controlling crystal fractionation paths. Mantle source compositions were estimated as binary mixtures of depleted mantle (North Atlantic Depleted Mantle or NADM) and small amounts of a hydrous fluid. We use their compositions for the NADM, the Azores Platform PREMA-type mantle source (AP), and the calculated Ti-bearing hydrous metasomatic fluid end-member AZ2 (main text Table S4-1), with modifications as described below. In their model, the mantle source for the Azores Platform PREMA-type basalts can be generated by addition of small quantities (0.3%) of AZ2 to NADM.

Asimow et al. [2004] interpret the origin of the enriched component as a small-degree partial melt of a partially dehydrated subducted slab. AZ2* trace element ratios Ba/Nb, Ba/La, and Ce/Pb are consistent with those for a 1% partial melt of subduction modified igneous crust (Figure S4-1 & 2) [*Cai et al.,* 2014]. *Cooper et al.* [2004] show that the small proportions of added

incipient melts are consistent with oxygen isotopic compositions and that the metasomatized mantle is capable of producing observed radiogenic isotopic compositions within ~250 Ma.

Concentrations of trace elements relative to H_2O are well constrained in the *Asimow et al.* [2004] model; however, the absolute concentrations are poorly constrained due to unresolved concentrations of major elements and other components (e.g., CO_2). Addition of major elements and other components will cause the overall abundance pattern of the enriched component to shift to lower concentrations, resulting in a complementary increase in the amount of that component needed to give the observed basalt compositions. On the mixing curves, this results in shifting end-member compositions along the mixing curve, but does not modify its curvature. Two important components excluded in the *Asimow et al.* [2004] analysis are carbon and chlorine. We use the recent results of *Kendrick et al.* [2017] to constrain Cl concentrations based on Cl/K ratios (for PREMA-type end-members Cl/K = 0.13 ±0.02, Cl/H_2O = 0.07). Estimating carbon concentrations is more complicated and is described below.

S4.2.2 Estimating carbonate concentrations in fluid compositions: The fact that the fluid composition considered above is fully hydrous is inconsistent with carbonatitic melt compositions predicted by experimental results of high pressure melting of carbonated eclogite, pelites and peridotites [e.g., *Dasgupta and Hirschmann*, 2006; *Kiseeva et al.,* 2012; *Grassi and Schmidt, 2011a and b*; *Thomson et al.*, 2016]. For well-justified reasons, experiments performed to explain arc processes have focused on the H_2O-dominated system, while those performed to explain deep mantle processes have focused the CO_2-dominated system. We need a mechanism to simultaneously constrain the proportions of H_2O and CO_2 of our incipient melts.

Diamonds provide a window into how much carbon might be expected in typical mantle C-O-H-Cl fluids. Researchers studying diamonds originating in the deep upper mantle and transition zone have long noted the affinity of host mineral inclusions to subducted oceanic crust and have advocated for the importance of interaction between ambient mantle and slab-derived carbonatitic fluids melts in their formation [e.g., *Shirey et al.,* 2013 and references therein; *Weiss et al.,* 2015; *Thomson et al.,* 2016]. Compositions of micro-inclusions in cloudy (inclusion-rich) diamonds are highly variable with three end-member compositions: (a) hydrous-silicic melt rich in water, (b) carbonatitic-melt rich in carbonate, and (c) saline fluids rich [e.g., *Navon et al.,* 1988; *Schrauder and Navon*, 1994; *Izraeli et al.,* 2001; *Klein-BenDavid et al.,* 2004, 2007]. All compositions are enriched in K and many other incompatible elements and are characterized by steep REE patterns similar to those in kimberlites and lamproites [*Schrauder et al.*, 1996; *Raga et al.,* 2003]. Water is always present in carbonatitic high-density fluids in diamonds [*Klein-BenDavid et al.*, 2007], with carbonate/(carbonate + water) molar ratios ranging from 0.5 to 0.7. These molar ratios are equivalent to CO_2/H_2O (by mass) of 2.5 to 6 (~4 ± 2).

Confirmation of primary magmatic CO_2/H_2O ratios in enriched oceanic basalts is hampered by near complete degassing of CO_2 during residence in the crust and eruption, but limited data suggests that CO_2/H_2O increases with enrichment in incompatible elements [*Michael and Graham,* 2015]. In highly depleted Siqueiros intra-transform spreading center, there is significantly less CO_2 than H_2O, with CO_2/H_2O by weight of 0.17 ± 0.02 [*Saal et al.,* 2002]. For enriched end-members, estimates of bulk volatile concentrations (dissolved in glass plus exsolved in vesicles) measured in highly vesicular basalts suggest that there is up to three times more CO_2 than H_2O in the sources for these basalts [*Sarda and Graham*, 1990; *Gerlach*,

1991; *Clague et al.*, 1991; *Dixon et al.,* 1991; *Dixon et al.,* 1997; *Dixon et al.,* 2002; *Cartigny et al.,* 2008], consistent with the lower end of the range determined from fluid inclusions in diamonds. For our models, we assume a CO_2/H_2O by weight of 2.0 in C-O-H-Cl fluid components near the upper range of calculated bulk volatile concentrations and the lower range of fluids in cloudy diamonds. In addition, we use the data of *Kendrick et al.* [2017] to constrain the Cl/K and Cl/H_2O in various mantle end-member components. For the endmembers described in the sections below, assuming a CO_2/H_2O of 2 results in CO_2 concentrations of 32.6 wt. % and 26.2 wt. % in the PREMA AZ2* and SYG* fluid components, respectively, and significantly lower concentrations of 10 wt. % and 1.8 wt. % in the DampEM and DryEM fluid components, respectively.

An alternate approach to predicting end-member fluid CO_2 concentrations is to use CO_2/Ba of 105 ± 9 [*Michael and Graham*, 2015]. Calculated CO_2 concentrations using CO_2/Ba of 105 yields 30.6 wt. % and 18.9 wt. % for the PREMA AZ2* and SYG* fluid components, respectively, and 69.8 wt. % and 7.6 wt. % in the DampEM and DryEM fluid components, respectively. Thus, there is significant uncertainty in the fluid CO_2 concentrations. An productive area of future research is to investigate if CO_2 concentrations in enriched end-members are coupled with H_2O, as is assumed in our model, or with Ba, as determined for MORB by [*Michael and Graham,* 2015].

Significant uncertainty in fluid CO_2 concentrations has insignificants impact on our modeled mantle compositions, however, as the main consequence of adding CO_2 to the fluid composition is to dilute all other component concentrations resulting in complementary increases in the fraction required to form the sources for enriched basalts. Therefore, uncertainty in CO_2 concentration in the C-H-O-Cl fluid does not impact the conclusions of this study and simply causes subtle adjustments in the amount of fluid added. For example, we use a H_2O concentration in the PREMA-type fluid (AZ2) in northern Atlantic of 28 wt. % (higher than the 21 wt.% calculated by *Asimow et al.* [2004]). If we add 2 times as much CO_2 by weight than H_2O, and 0.07 as much Cl than H_2O, and renormalize to 100 %, the revised C-H-O-Cl composition (AZ2*) has 16 wt. % H_2O and 33 wt. % CO_2. Because the amount of water (and all other components) has been reduced by roughly 40 % compared to the hydrous-only composition, the amount of fluid required to produce the observed enriched compositions will need to be increased by about 70%. For the Azores Platform, the required amount of AZ2* component increases from 0.31 % to 0.52 % resulting in a mantle source for the most enriched Azores Platform basalts of 896 ppm H_2O and 1703 ppm CO_2. Uncertainty in carbon concentrations by about a factor of 2 results in similar levels of uncertainty in the proportion of C-O-H-Cl fluid needed to produce the observed enriched basalt compositions.

In Table S4-1, we show both the hydrous-only AZ2 and C-H-O-Cl AZ2* compositions for the Azores Platform. We reiterate that the trace element concentrations relative to H_2O were determined by a polybaric hydrous melting and fractionation model that honors all available data, including major element and trace compositions of primary and differentiated magmas, extent of melting, and crustal thickness.

S4.2.3 Results of binary NADM-AZ2* mixing models for the Azores Platform: Mixing curves for Azores Platform basalts are shown in the main text Figures 2a through d. The depleted mantle end-member (NADM) containing 50 ppm H_2O and H_2O/Ce of 200 [*Asimow et al.,* 2004] must have extremely light hydrogen isotopic values (δD_{SMOW} = -135 ‰) to fit the Azores Platform basalt data. For the Azores PREMA C-H-O-Cl fluid mixing end-member (AZ2*), we use a H_2O

concentration of 16 wt. %, 33 wt. % CO_2, 11 wt. % Cl, H_2O/Ce of 286, and a δD_{SMOW} of -40 ‰. The mantle source for the most enriched Azores Platform basalts (AP; $^{206}Pb/^{204}Pb$ of 19.7), formed by addition of 0.52% AZ2* to NADM, has 900 ppm H_2O, 1700 ppm CO_2, 60 ppm Cl, H_2O/Ce of 279, and -45 ‰ δD_{SMOW}. The mantle source for average North Atlantic MORB ($^{206}Pb/^{204}Pb$ of 18.5 ± 0.1), formed by addition of ~ 0.03 ± 0.01 % AZ2* to NADM, has roughly 100 ± 20 ppm H_2O, 110 ± 41 ppm CO_2, 5 ± 1 ppm Cl, H_2O/Ce of 235 ± 8, and δD_{SMOW} = -88 ± 7 ‰.

To fit the Li data, we estimate δ^7Li values of 3.0 and 5.1 for NADM and AZ2*, respectively. The heavier δ^7Li for the AZ2* PREMA-type end-member is consistent with previous results [*Elliott et al.,* 2006; *Krienitz et al.*, 2012], who showed that HIMU (PREMA)-type lavas are characterized by δ^7Li values up to +4.8‰, which they interpreted as being due to recycling of altered and dehydrated oceanic crust.

S3.2.4 Arctic EM-type end-member (WetEM): Though significantly depleted in incompatible elements compared to Jan Mayen basalts, Mohns Ridge basalts have elevated $^{87}Sr/^{86}Sr$ and Ba/Nb at unradiogenic $^{206}Pb/^{204}Pb$ compared to depleted MORB south of the Azores Platform, consistent with involvement of an EM-type component. Based on the similarity in trace element ratios, such as Ba/Nb, Ba/La, H_2O/Ce and Ce/Pb, between EM-type mantle sources and subduction components for hot slabs (Figures S4-1 & 2) [e.g., *Ruscitto et al.,* 2012; *Cai et al.,* 2014], we investigate the feasibility of using carbonated sediment and/or crustal melts as end-members as mixing end-members for observed EM compositions. This approach assumes that there are not significant compositional changes associated with sediment melting in Zone 1.

We calculated simple binary mixing of source compositions, utilizing Ba, Nb, La, H_2O, Ce, Pb, Sr, and Sm concentration data for subduction components [*Ruscitto et al.*, 2012] and for depleted mantle [*Asimow et al.*, 2004]. We find that the Jumiltepec (Mexico) hydrous component [*Ruscitto et al.,* 2012] provides a suitable fit for trace elements and H_2O (WetEM), although the [Ba] was increased to better fit the data. Because the compositions of modern arc end-member components have not yet "aged" to produce the radiogenic isotopic compositions attained by their ancient analogs, radiogenic isotopic compositions in the subduction mixing end-members were estimated to fit the data. We use the observed range in EM end-member radiogenic isotopic compositions [e.g., *Stracke,* 2012] to estimate $^{87}Sr/^{86}Sr$ of ~0.7038 and $^{206}Pb/^{204}Pb$ of 17.3 for our Arctic WetEM end-member. Other studies have shown that mantle metasomatized by small amounts of carbonated pelite melt melts is capable of evolving into observed EM-type radiogenic isotopic compositions [e.g., *Grassi et al.*, 2012].

Our calculated WetEM C-H-O-Cl fluid has 18.1 wt. % H_2O, 36.3 wt. % CO_2, 13 wt. % Cl, H_2O/Ce of 574, and δD_{SMOW} of -37 ‰. The EM-influenced Mohns Ridge mantle (M) can be produced by adding just a trace (0.04 %) of WetEM to the NADM resulting in 123 ppm H_2O, H_2O/Ce of 326, and δD_{SMOW} of -77 ‰. The depleted end of the Mohns Ridge array has roughly 1/3 of its water from NADM (δD_{SMOW} of -135 ‰) and 2/3 from the WetEM (δD_{SMOW} of -37 ‰) yielding δD_{SMOW} = -77 ‰. Gradients in trace element and radiogenic and stable isotopic compositions along the Mohns Ridge represent mixing between the PREMA-type Jan Mayen (JM) and EM-type Mohns mantle components. Measured Ba/Nb and H_2O/Ce in many basalts, especially near the Jan Mayen plume, are greater than the modeled values and may be due to increases in these ratios due to low extents of partial melting or to assimilation of seawater or brines.

S4.2.5 Jan Mayen PREMA-type end-member: The Jan Mayen mantle source (JM) can be modeled by mixing between Mohns and AZ2* end-members (JM = 99.69%Mohns + 0.31%AZ2*). We use δD_{SMOW} of -30 ‰ for the AZ2* end-member, which is heavier by ~10 ‰ than the value used for the Azores Platform model because of the ~10 ‰ offset between the conventional (Arctic) and TC/EA (Azores Platform) δD_{SMOW} data. The mantle source for the most enriched Jan Maayen basalts (JM; [206]Pb/[204]Pb of 18.9), formed by addition of 0.31% AZ2* to the Mohns source, has 630 ppm H_2O, 1020 ppm CO_2, 40 ppm Cl, H_2O/Ce of 293, and -38.4 ‰ δD_{SMOW}.

S4.3 Pacific and southern Atlantic PREMA-type endmember

S4.3.1 Salas y Gomez PREMA-type end-member: Unlike the Azores Platform, a comprehensive mantle composition and melt generation model is not available for the Easter Microplate – Easter Salas y Gomez Seamount Chain (EMP-ESC) system, though mantle source compositions for the most enriched basalts have been estimated for a few elements (La, H_2O, Ce, and Cl) [*Simons et al.,* 2002]. To successfully model the Pacific data, the depleted end-member for Pacific basalts (PacDM) must be slightly more depleted in the most incompatible elements (Ba, Nb) compared to NADM, consistent with other results [*Arefalo & McDonough*, 2010]. We assumed mantle concentration of H_2O was similar to the NADM, and calculated the concentrations of other elements using iterative forward modeling to generate trace element ratios observed in the basalts. Our PacDM has 50 ppm H_2O, 4 ppm CO_2, 1 ppm Cl, H_2O/Ce of 140, and δD_{SMOW} of -95 ‰.

EMP-ESC basalts are distinct from Azores Platform basalts with lower Ba/Nb, Ba/La, H_2O/Ce, La/Sm, and [87]Sr/[86]Sr at a given [206]Pb/[204]Pb. Compared to the Atlantic PREMA C-H-O-Cl component (AZ2*), the Pacific PREMA C-O-H-Cl component (SYG*) is shifted to higher [206]Pb/[204]Pb and lower [87]Sr/[86]Sr and Ba/Nb. This difference is consistent with contribution of an EM-like component to the Atlantic upper mantle. For the SYG* C-H-O-Cl fluid end-member, we arbitrarily pinned the Ce concentration (570 ppm) to be consistent with that of the AZ2 C-O-H-Cl fluid, used CO_2/H_2O of 2.0, and Cl/H_2O of 0.05. Concentrations of other elements were estimated by iterative forward modeling based on correlations between a variety of trace element and radiogenic isotopic ratios resulting in a SYG* fluid with 13 wt. % H_2O, 26 wt. % CO_2, 0.66 wt. % Cl, H_2O/Ce of 230, and δD_{SMOW} of -38 ‰. Binary mixing of mantle components for the EMP-ESC system are shown on Figures 3a through d in the main text.

Average Pacific MORB mantle can be modeled as PacDM plus a trace (~ 0.04 ± 0.01 %) of the SyG* fluid component resulting in about 102 ± 15 ppm H_2O, 110 ± 35 ppm CO_2, 4 ± 1 ppm Cl, H_2O/Ce from 180 ± 15, and δD_{SMOW} of -66 ± 4 ‰ at a [206]Pb/[204]Pb of 18.33, consistent with average values observed along the EPR and PAR. Below, these mantle compositions are referred to as AvgEPR1 (+0.03 % SYG*; 89 ppm H_2O; [206]Pb/[204]Pb = 18.22; δD_{SMOW} of -70 ‰) and AvgEPR2 (+0.04 % SYG*; 102 ppm H_2O; [206]Pb/[204]Pb = 18.33; δD_{SMOW} of -66 ‰), consistent with previously determined values for the average Pacific MORB source (~120 ± 27 ppm H_2O, 4.5 ±1.4 ppm Cl, H_2O/Ce of 150 ± 10, and δD_{SMOW} of -65 ‰) [*Kingsley et al.,* 2002; *Simons et al.,* 2002].

Addition of 0.66 % SyG* to PacDM produces the mantle source composition for the most enriched ESC basalts. This Pacific PREMA-type mantle source (SYG) has 915 ppm H_2O, 1740 ppm CO_2, 45 ppm Cl, H_2O/Ce of 223, and δD_{SMOW} of -41 ‰, consistent with previously

determined values for the SYG mantle source (750 ± 210 ppm H_2O, 36 ± 10 ppm Cl, H_2O/Ce of 210 ± 10, and δD_{SMOW} of -35 ‰) [*Kingsley et al.,* 2002; *Simons et al.,* 2002]. To fit the $\delta^{11}B$ data, our calculated AvgEPR1 mantle has 0.11 ppm B and $\delta^{11}B$ of -8.5 ‰ consistent with accepted MORB source [B] and $\delta^{11}B$ values [*Chaussidon and Jambon*, 1994; *Chaussidon and Marty*, 1995; *Ryan and Langmuir*, 1993]. We estimate the SYG* component to have ~140 ppm B and $\delta^{11}B$ of +10 ‰ consistent with $\delta^{11}B$ for serpentine of +8 to +13.0 ‰ [*Spivack and Edmond,* 1987; *Benton et al.,* 2001]. *Gurenko and Kamentsky* [2011] document mixing, defined by olivine-hosted melt inclusions in Gorgona komatiites, of mantle and a B-rich subduction-related fluid with $\delta^{11}B$ of >+10 ‰.

S4.3.2 South Atlantic EM-type end-member: Mixing curves for the EMP-ESC and southern MAR basalts are shown on Figures 4a through d in the main text. To fit the Discovery data, we assumed a Sm concentration of 35 ppm in the EM fluid component and solved iteratively to determine the other elements. We refer to this component as DampEM component because the water content and H_2O/Ce (5.0 wt. %, 100) are significantly less than that needed for the northern Atlantic WetEM component (34 wt. %, 286). We reiterate that if we selected a different Sm concentration, it would impact the amount of fluid added to generate a similar enriched mantle source. The mantle source for the most enriched Discovery anomaly basalts is formed by addition of 0.23 % of the DampEM fluid component to AvgEPR1 resulting in a mantle source for the most enriched Discovery anomaly basalts with 204 ppm H_2O, 310 ppm CO_2, 6.7 ppm Cl, H_2O/Ce of 122, and δD_{SMOW} of -69 ‰. To fit the $\delta^{11}B$ data, we estimate the DampEM component to have ~400 ppm B and $\delta^{11}B$ of -6.6 ‰ consistent with dehydrated sediments (-1 to -8 ‰) [*Ishikawa and Nakamura*, 1993]. The Discovery mantle source is calculated to have 1 ppm B and $\delta^{11}B$ of -6.4 ‰.

S4.3.3 Northern EPR EM-type end-member: Mixing curves for the EMP-ESC and northern EPR basalts are shown on Figures 5a through 5d in the main text. Analogous to the procedure for the southern Atlantic, we assume that the middle REE (Sm) is similar to the DampEM component and solved iteratively to determine the other elements. We refer to this component as the DryEM component because the water content (1.1 wt. %) is significantly less than that needed for both the DampEM (5.0 wt. %) and WetEM components (34 wt. %). The estimated DryEM fluid component has 0.9 wt. % H_2O, 17.6 wt. % CO_2, 330 ppm Cl, H_2O/Ce of 76, and δD_{SMOW} of -125 ‰. The mantle source for the most enriched EM-like northern EPR basalts is formed by addition of 1 wt. % of the DryEM C-O-H-Cl fluid component to AvgEPR1 resulting in a mantle source with 190 ppm H_2O, 280 ppm CO_2, 6.5 ppm Cl, H_2O/Ce of 110, and δD_{SMOW} of -99 ‰.

While estimated fluid end-member compositions are non-unique, the proportions of elements relative to H_2O are tightly constrained by trends in magma composition. As an example, an alternate approach to that described above is to assume that the DryEM component has a Ba concentration similar to that in the DampEM fluid (6650 ppm instead of 720 ppm). Using this assumption, the concentrations of all elements would need to be increased by nearly an order of magnitude (9.24X) and the amount of fluid required to produce the enriched EM-like EPR basalts would be reduced to 0.11 wt. %. The DryEM fluid component calculated using Ba = 6650 ppm has 8.1 wt. % H_2O, 16.2 wt. % CO_2, 3085 ppm Cl, H_2O/Ce of 76, and δD_{SMOW} of -125 ‰. In this case, DryEM fluid H_2O concentration (8.1 wt. %) is greater than that in the DampEM fluid (5.0 wt. %). The term "Dry" should be considered as dry in a relative sense compared to Ce (lower H_2O/Ce), as originally applied in *Dixon and Clague* [2001] and *Dixon et al.* [2002]. The

mantle source for the most enriched EM-like northern EPR basalts, formed by addition of 0.11 wt. % of this alternate DryEM C-O-H-Cl fluid component to AvgEPR1, results in a mantle source identical to that listed above.

In other words, changing the absolute concentration of the fluid end member by an order of magnitude results in a complementary decrease by an order of magnitude in the amount of end member required to produce the observed mantle source, but does not change the key trends in mantle and magmatic trace element and isotopic ratios.

S4.4 Predicted magma compositions

To test the validity of our estimated enriched mantle sources, we calculated magma compositions for the Arctic Ridges, the Azores Platform, and the EMP-ESC regions. Parental magma compositions are calculated using simple batch melting:

$$c_m = \frac{c_s}{(F + D^*(1-F))}$$ (eqn. S4.3),

where c_m is the concentration in the melt, c_s is the concentration in the mantle source, F is the extent of melting, and D^* is the bulk distribution coefficient. For the MORB end-member, we used bulk distribution coefficients from *Workman and Hart* [2005]. For the enriched end-member, 1-5 % garnet was added to the source using garnet distribution coefficients from *Salters et al.* [2002]. Distribution coefficients are listed in Table S4.2. For each area, the extent of melting decreases from the depleted to enriched source regions due to the large volume of deep mantle that experiences small degrees of hydrous and carbonated melting in the enriched sources [*Asimow et al.*, 2004]. Mantle sources are calculated as binary mixtures of the Mohns and JM sources for the Arctic Ridges, the NADM and AP sources for the Azores Platform, and the AvgEPR2 and SYG sources for the Easter system. Extents of melting are calculated as a function of the fraction of the enriched component in the source, and range from 1 - 12 % for the Arctic Ridges, 5 – 8 % for the Azores Platform, and 7 – 12 % for the EMP-ESC. Calculation of parental magmas in these hydrous systems is complicated by the role of H_2O in controlling the fractionating mineral assemblage. We accounted for fractional crystallization by treating elements as perfectly incompatible and calculating curves for 10 – 50 % fractional crystallization. Model results compared to observed compositions for basalts with MgO > 7.0 wt. % are shown on Figures S4-4 to S4.6. Though the details of extents of melting and fractional crystallization may shift with more sophisticated modeling, this simple model shows that our estimated mantle compositions provide plausible sources for the observed basalts.

S4.5 Summary

EM and PREMA mantle sources can be successfully modeled by addition of small amounts (<1%) of incipient melts. End-member fluid compositions are shown as a function of H_2O/Ce (Figure S4-3). PREMA end-members (AZ2* and SYG*) have a narrow range in δD_{SMOW} that is similar to that for antigorite (serpentine). EM-type end-members have variable δD_{SMOW}. All sediments should be dehydrated by 80 – 120 km depth [*van Keken* et al., 2011]. Low H_2O/Ce and light δD_{SMOW} in the estimated DryEM fluid are consistent with near complete dehydration. Higher H_2O/Ce and heavier δD_{SMOW} in the Damp and DryEM fluids are consistent with reequilibration with unfractionated subcrustal hydrous phase fluids from deeper cooler

portions of the slab. Ba/Nb, Ba/La, and Ce/Pb of DampEM and DryEM are intermediate between estimates of shallow hot slab fluids [*Ruscitto et al.,* 2012] and of deep igneous crustal melts [e.g., *Stracke et al.*, 2003; *Cai et al.,* 2014] and may be related to progressive extraction of fluids and melts from the slab materials.

We argue that metasomatism from slab-derived fluids provides a reasonable alternative to than models involving wholescale mixing of subducted lithologies or autometasomatism (with melts or fluids from ambient mantle). Subduction-related metasomatic models have been previously advocated [e.g., *Asimow et al.*, 2004; *Cooper et al.*, 2004; *Donnelly et al.,* 2004; *Weiss et al.,* 2016], but autometasomatic models are more common in the literature [e.g., *McKenzie and O'Nions*, 1983, 1995; *Roden et al.,* 1984; *Galer and O'Nions,* 1986; *Halliday et al.,* 1995; *Niu et al.,* 2002; *Niu and O'Hara*, 2003; *Workman et al.,* 2004]. For example, *Willbold and Stracke* [2006] estimated mantle end-member compositions and provided families of permissible trace element patterns as a function of source mineralogy, partition coefficients, and degree of melting. They interpreted trace element concentrations in terms of direct mixing of various subduction lithologies, but models involving metasomatism of depleted mantle by partial melts of subducted lithologies were not considered, mainly because of the absence of a thermodynamic mechanism that could reliably produce incipient melts of downgoing slabs. Our model provides a previously unrecognized mechanism to generate these incipient melts. *Workman et al.* [2004] present a model for the EM2 source for Samoa and argued for the autometasomatism model rather than involvement of subduction lithologies. Stable isotopic values measured in this study require involvement of surface-modified materials and are inconsistent with the autometasomatism hypothesis.
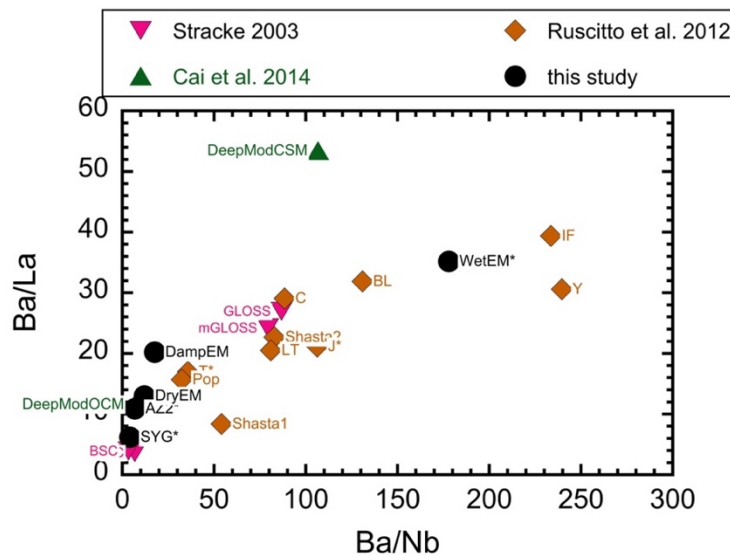
Figure S4-1. Comparison of trace element ratios for calculated end-member compositions compared to other subduction-related materials. Brown diamonds are hot slab components [*Ruscitto et al.,* 2012]; BIC and BSC are Bulk Igneous Crust and Bulk Modified Subducted Crust [*Stracke et al.,* 2003]; GLOSS and mGLOSS are global sediment averages [*Plank and Langmuir,* 1998]; DeepModOCM and DeepModCSM are calculated 1% melt of subduction-modified ocean crust formed under eclogite-only mineralogy (no accessory phases) and a composite of 1% deep eclogite + 5% deep sediment melt [*Cai et al.,* 2014]. Our PREMA-type AZ2* is similar to DeepModOCM. WetEM is modeled after the Jumiltepec hot slab component. DampEM and DryEM compositions are intermediate between AZ2* and Wet EM.
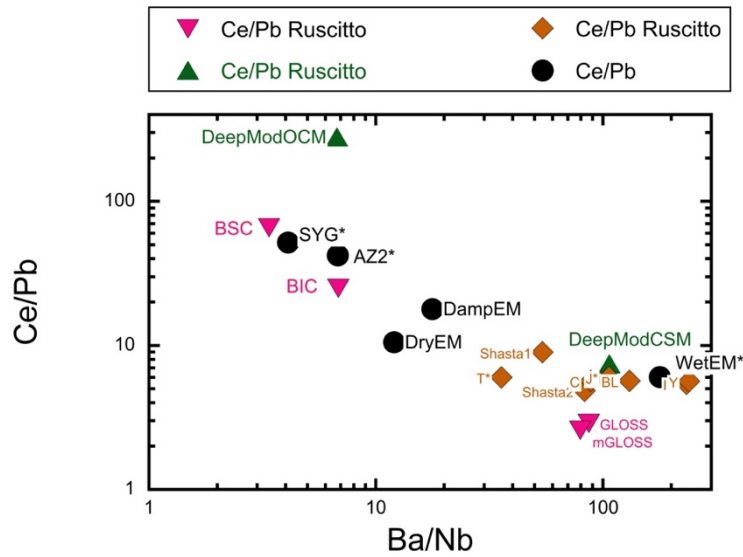
Figure S4-2. Similar to S4-1, for Ce/Pb.
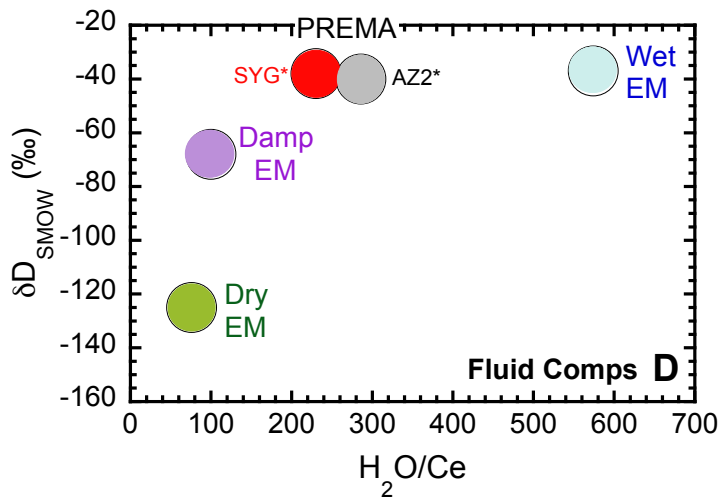
Figure S4-3. Summary of calculated C-H-O-Cl fluid end-member compositions showing limited range in H_2O/Ce and δD_{SMOW} for PREMA-type end-members compared to variable EM-type compositions.

(Figure S4.4 – Mohns – Jan Mayen mixing, melting, fractional crystallization)
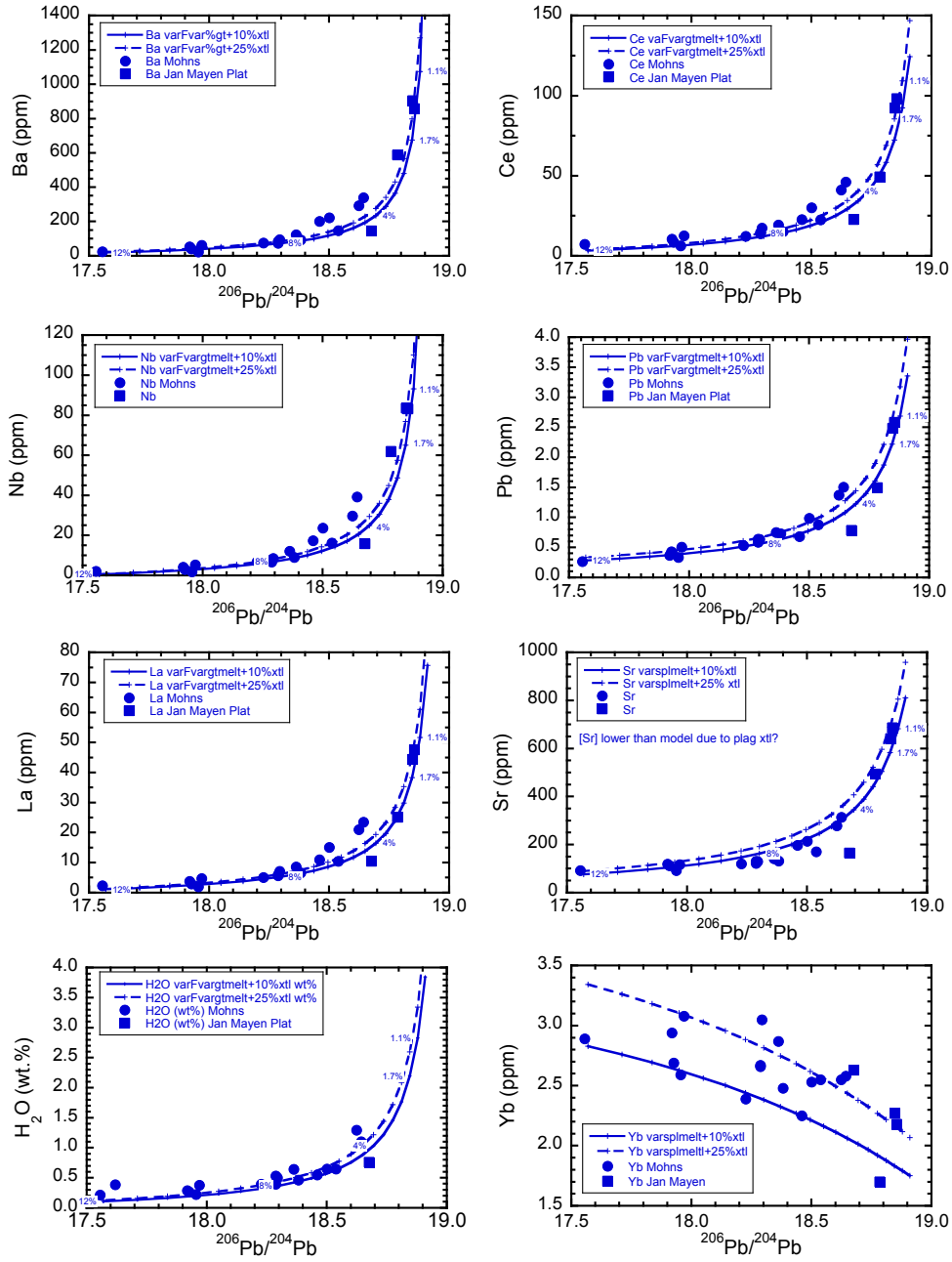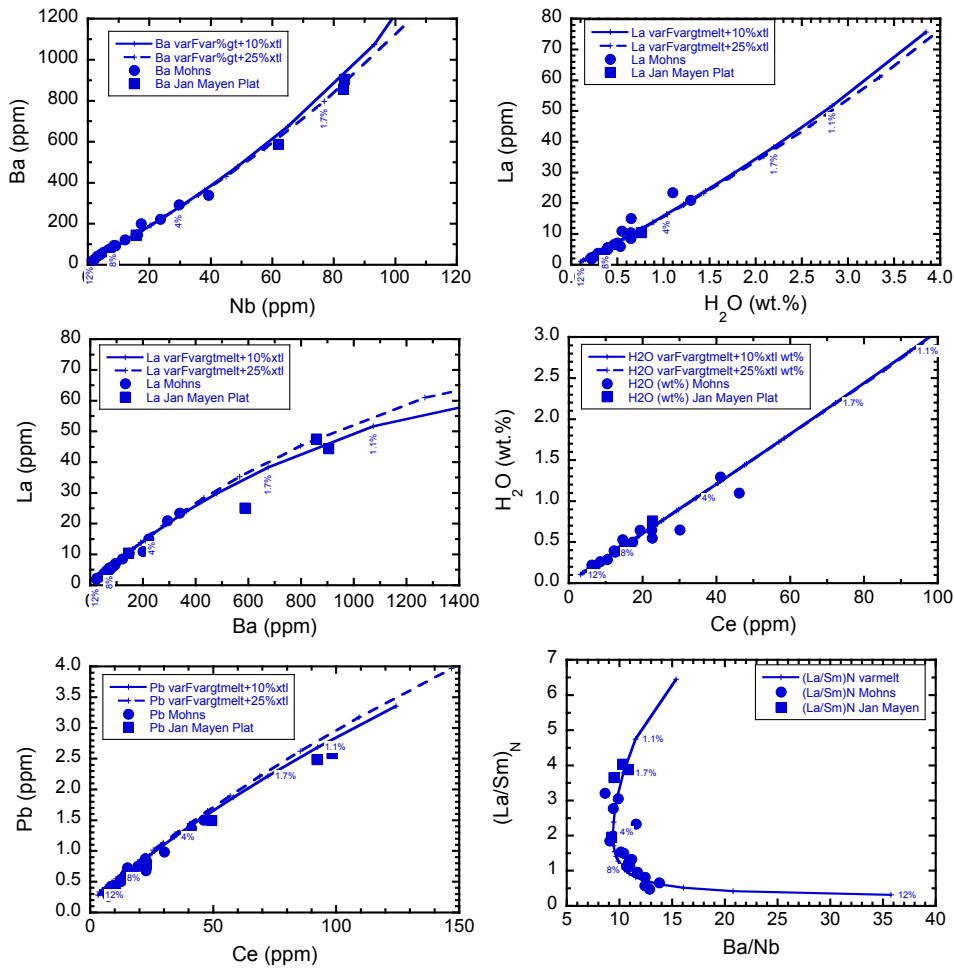
Figure S4.4. Elemental concentrations for Mohns Ridge and Jan Mayen basalts with MgO > 7 wt. %. Mantle composition was calculated as a binary mixture of the Mohns (M) and Jan Mayen (JM) sources (Table S4.1). Extents of partial melting vary from ~1.5 % for the most enriched Jan Mayen basalts to ~12 % for the most depleted Mohns Ridge basalts and decrease as the proportion of the JM end-member increases. Previous work [*Neumann and Schilling*, 1984] interpreted low HREE concentrations in Jan Mayen platform lavas as being caused by melting within the garnet lherzolite mineral field. The amount of residual garnet is estimated to increase from zero for the depleted Mohns end-member to 5 % at the enriched Jan Mayen end-member. The average MgO for Mohns Ridge basalts is 8.0 ± 0.7 wt. %, thus we bracketed our results with 10 to 25 % fractional crystallization. H_2O concentrations could not be measured in the most enriched Jan Mayen basalts due to degassing and devitrification, however, our model suggests that those melts should contain roughly 2.5 wt. %. H_2O.

(Figure S4.5 – Azores Platform mixing, melting, fractional crystllization)
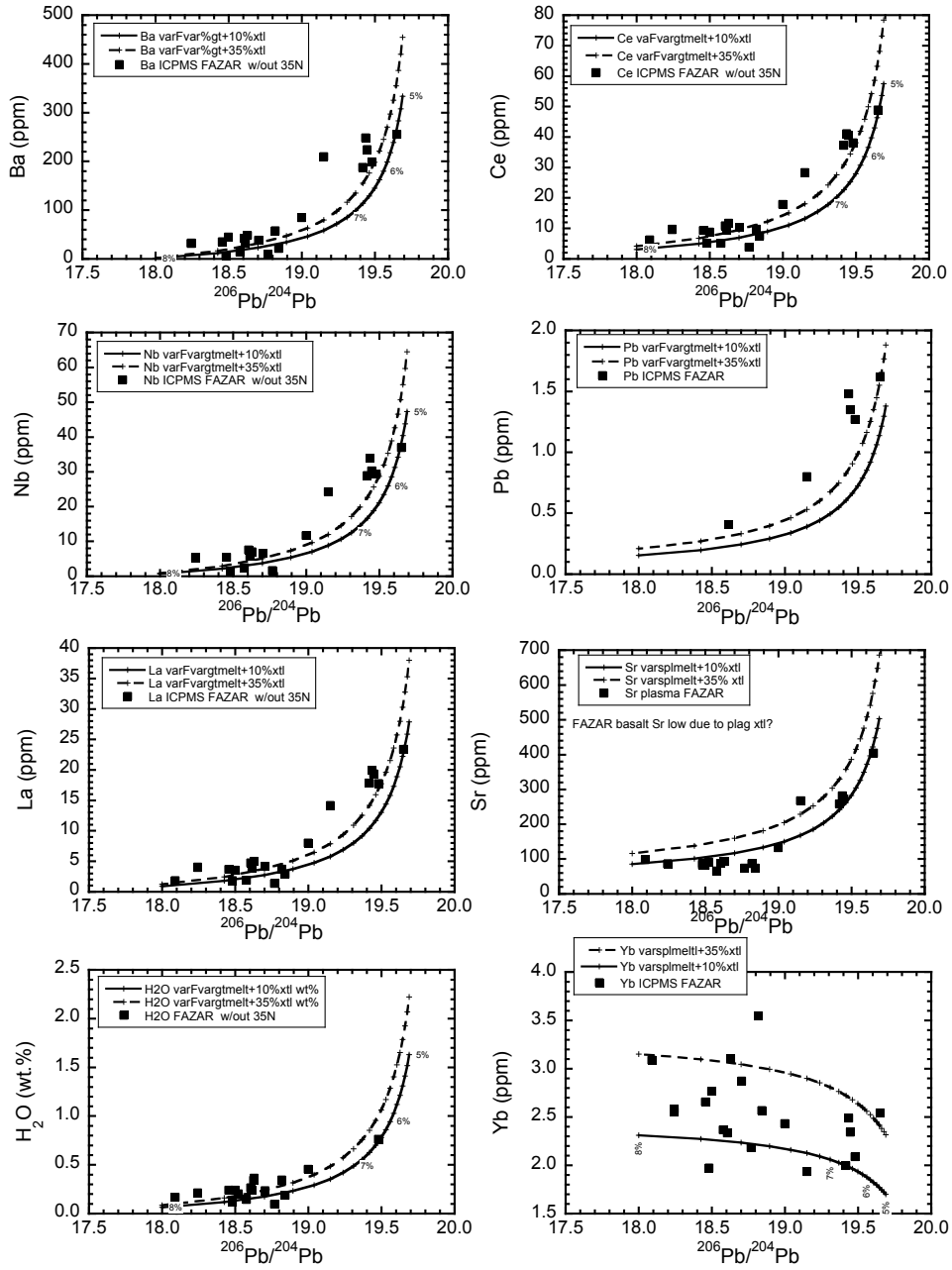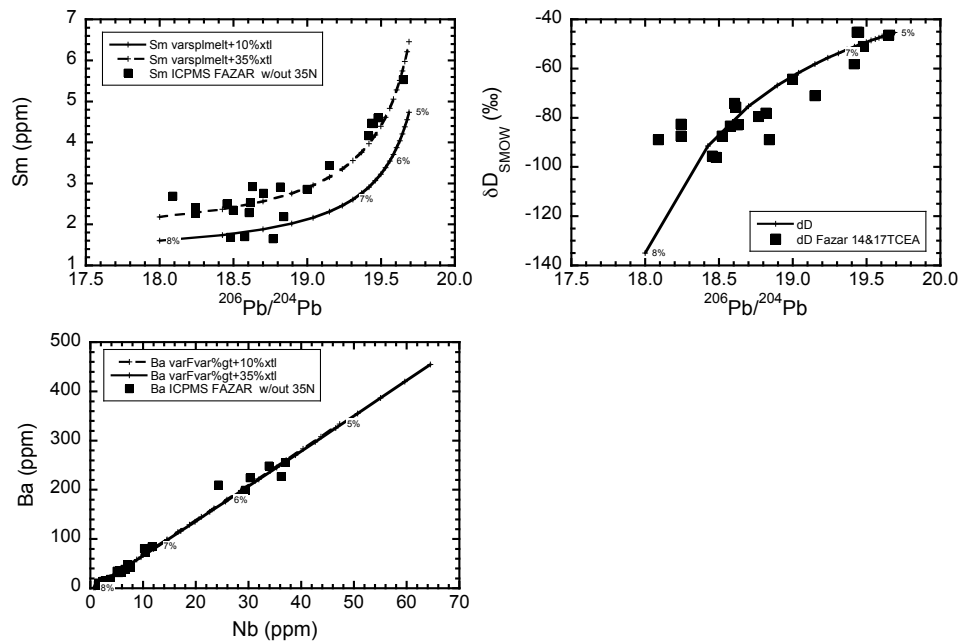
Figure S4.5. Elemental concentrations for Azores Platform basalts with MgO > 7 wt. %. Mantle composition was calculated as a binary mixture of the north Atlantic depleted mantle (NADM) and the Azores Platform (AP) sources (Table S4.1). Extents of partial melting vary from ~5 % for the most enriched Azores Platform basalts to ~8 % for the most depleted mid-Atlantic Ridge basalts and decrease as the proportion of the AP end-member increases. The amount of residual garnet is estimated to increase from zero for the depleted MAR end-member to ~1 % at the enriched Azores Platform end-member. Azores Platform basalts have slightly lower average MgO contents than Arctic Ridge basalts, thus we bracketed our results with 10 to 35 % fractional crystallization. H_2O concentrations in the most enriched Azores Platform basalts should be roughly 1.5 to 1.8 wt. % prior to degassing.

(Figure S4.6 – EMP-ESC mixing, melting, fractional crystallization)
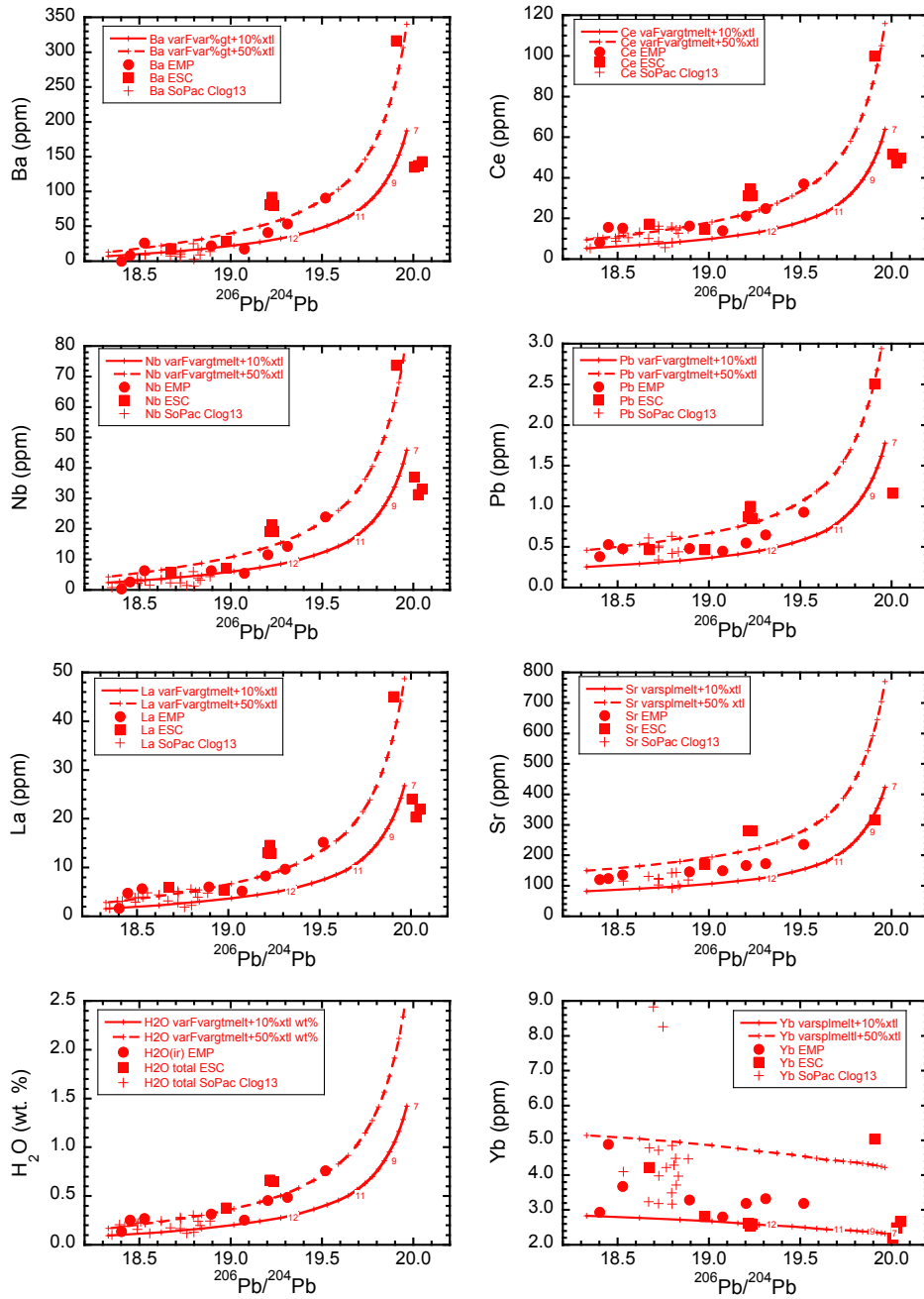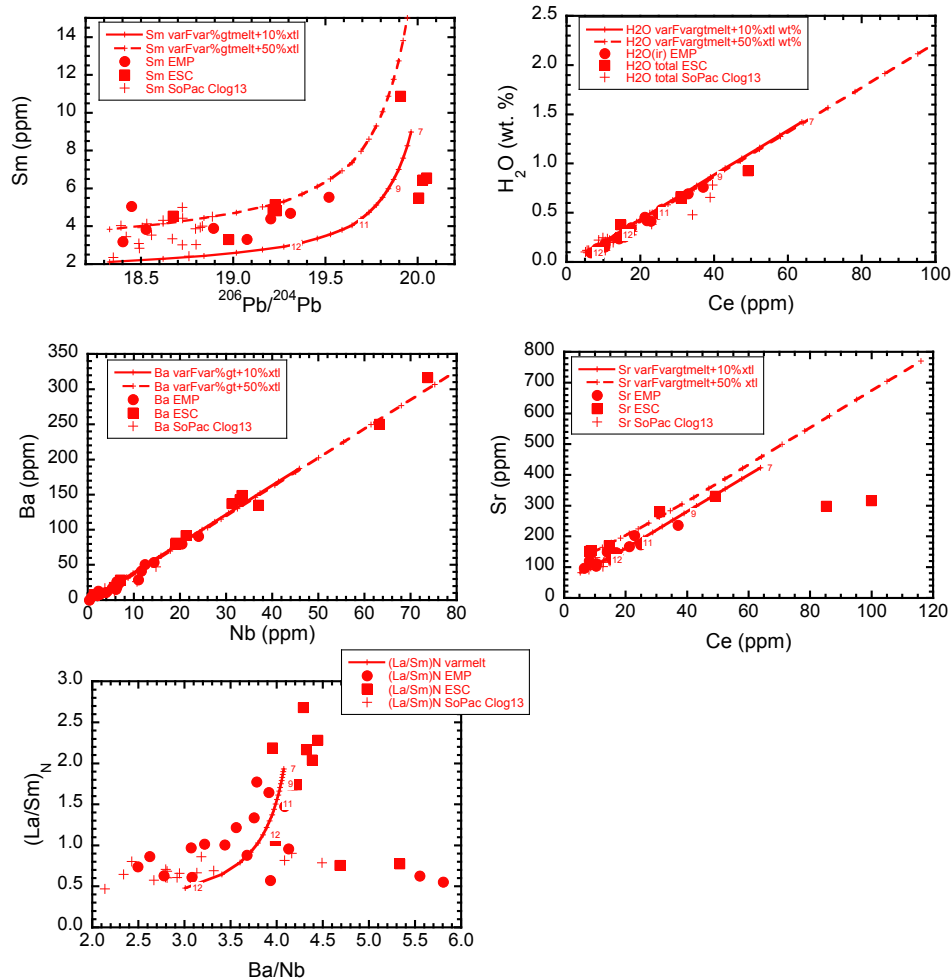
Figure S4.6. Elemental concentrations for EMP-ESC basalts with MgO > 7 wt. %. Mantle composition was calculated as a binary mixture of the Pacific depleted mantle (PacDM) and the Salas y Gomez Seamount Chain (SYG) sources (Table S4.1). Extents of partial melting vary from ~7 % for the most enriched SYG seamount chain basalts to ~12 % for the most depleted EPR basalts and decrease as the proportion of the SYG end-member increases. In this case there is a sharper transition such that the seamount chain basalts are all produced by less than 10 % melting. The amount of residual garnet is estimated to increase from zero for the depleted EPR end-member to ~1 % at the enriched SYG end-member. EPR and ESC basalts have slightly lower average MgO contents than Arctic Ridge and Azores Platform basalts, thus we bracketed our results with 10 to 50 % fractional crystallization. H_2O concentrations in the most enriched Salas y Gomez seamount chain basalts should be roughly 1.5 to 2.0 wt. % prior to degassing.

Table S4-1: Mixing End-members (See text for explanation)

Element	NADM North Atlantic Depleted Mantle [Asimow et al., 2004]	AZ2 Azores Platform PREMA Hydrous [Asimow et al., 2004]	AZ2* Azores Platform PREMA C-H-O-Cl	AP Source for most enriched Azores Platform basalts **AP**=0.9948NADM + 0.0052AZ2*	AvgNMAR =0.9997NADM +0.0003AZ2*
Ba	0.10	5000	2910	15.2	0.97
Nb	0.05	740	430	2.3	0.18
CO_2*	10	-	325,600	1703	108
Cl*	1.5	-	11,400	61	4.9
La	0.07	460	267	1.46	0.15
H_2O	50	2.80E+05	162,800	896	99
Ce	0.25	980	570	3.21	0.42
Pb	0.013	23.2	13.5	0.083	0.017
Sr	8	8800	5120	34.6	9.5
Sm	0.17	92	53	0.44	0.19
Yb	0.24	0	0	0.24	0.24
Li*	0.03	-	34.7	0.22	0.04
$^{87}Sr/^{86}Sr$	0.7026	0.7038	0.7038	0.7035	0.7028
$^{206}Pb/^{204}Pb$	18.00	20.00	20.00	19.69	18.48
δD_{SMOW} (‰)	-135	-40 / -30	-40	-45.3	-88
δ^7Li (‰)	2.9	-	5.1	4.8	3.4
Ba/Nb	2	6.8	6.8	6.7	5.44
Ba/La	1.4	10.9	10.9	10.4	6.48
H_2O/Ce	200	286	286	279	235
H_2O/La	714	609	609	615	658
$(La/Sm)_N$	0.27	3.2	3.2	2.11	0.52
Ce/Pb	19.2	42.2	42.2	38.8	24.7
CO_2/Nb	200	-	757	744	600
CO_2/H_2O	0.20	-	2.0	1.9	1.09
CO_2/Ba	100		112	112	111
Cl/H_2O	0.03	-	0.07	0.068	0.67

Table S4-1 cont.

Element	NADM North Atlantic Depleted Mantle [*Asimow et al.*, 2004]	WetEM Hydrous Jumiltepec [*Ruscitto et al.*, 2012]	WetEM C-H-O-Cl Arctic	M Mohns = 0.9996NADM +0.0004*Wet EM	JM Jan Mayen **JM=0.9969M + 0.0031AZ2***
Ba	0.10	5678	5069*	2.13	11.1
Nb	0.05	53.4	28.5	0.061	1.39
CO_2*	10	-	362,860	155	1019
Cl*	1.5	25,321	12,700	6.6	42
La	0.07	269	144	0.13	0.96
H_2O	50	395000	181,430	123	627
Ce	0.25	592	316	0.38	2.14
Pb	0.013	98	52.3	0.034	0.076
Sr	8	8753	4671	9.9	25.7
Sm	0.17	59	375	0.32	0.48
Yb	0.24	0	855	0.58	0.578
Li*	0.03	-	-	-	-
$^{87}Sr/^{86}Sr$	0.7026	0.7043	0.7038	0.7030	0.70342
$^{206}Pb/^{204}Pb$	18.00	17.30	17.30	17.53	18.91
δD_{SMOW} (‰)	-135	-37	-37	-72.5	-38.4*
δ^7Li (‰)	2.9	-	-	-	-
Ba/Nb	2	106	178	41.0	8.0
Ba/La	1.4	21.1	35.2	18.6	11.7
H_2O/Ce	200	667	574	345	276
H_2O/La	714	1468	1260	1007	617
$(La/Sm)_N$	0.27	2.94	2.95	0.49	1.81
Ce/Pb	19.2	6.04	6.04	10.4	37.2
CO_2/Nb	200	-	12,732	2541	733
CO_2/H_2O	0.20	-	2.0	1.3	1.9
CO_2/Ba	100	-	71.6	72.7	91.5
Cl/H_2O	0.03	0.06	0.07	0.056	0.67

Table S4-1 cont.

Element	PacDM Pacific DMM	SYG* Pacific PREMA	SYG =0.9934*PacDM+0.0066*SYG*	AvgEPR1 = 0.9997PacDM +0.0003SYG*	AvgEPR2 = 0.9996PacDM +0.0004SYG*
Ba	0.05	180	11.9	0.59	0.77
Nb	0.09	430	2.93	0.22	0.26
CO_2*	4	262200	1735	83	109
Cl*	1.3	6,554	44.5	23.27	3.9
La	0.12	250	1.77	0.20	0.22
H_2O	50	131,000	915	89	102
Ce	0.35	570	4.11	0.52	0.58
Pb	0.023	14	0.115	0.027	0.028
Sr	8	3000	27.7	8.9	9.2
Sm	0.21	60	0.60	0.23	0.23
Yb	0.58	0	0.58	0.58	0.58
B*	0.05	140	0.84	0.11	0.12
$^{87}Sr/^{86}Sr$	0.70222	0.7036	0.70326	0.70239	0.70244
$^{206}Pb/^{204}Pb$	17.8	20.5	19.965	18.217	18.33
δD_{SMOW} (‰)	-95	-38	-41.4	-69.9	-65.8*
$\delta^{11}B$ (‰)	-12	+10	+7.6	-6.4	-
Ba/Nb	0.56	4.2	4.08	2.69	3.4
Ba/La	0.42	7.2	6.75	3.03	3.8
H_2O/Ce	140	230	223	168	183
H_2O/La	500	524	517	510	514
$(La/Sm)_N$	0.30	2.69	1.89	0.49	0.67
Ce/Pb	19.2	40.7	35.7	24	27.5
CO_2/Nb	44	610	645	486	710
CO_2/H_2O	0.08	2.0	1.9	0.93	1.55
CO_2/Ba	80	146	146	141	69
Cl/H_2O	0.03	0.05	0.05	0.037	0.041

Table S4-1 cont.

Element	AvgEPR1 = 0.9997PacDM +0.0003SYG*	DampEM	Discovery D = 0.9977EPR1 + 0.0023DampEM	DryEM	NoEPR E = 0.99EPR1 + 0.01DryEM
Ba	0.59	6650	15.8	720	7.96
Nb	0.22	375	1.08	60	0.86
CO_2*	83	100,000	313	17600	284
Cl*	3.3	1500	6.7	334	6.52
La	0.20	330	0.95	56	0.78
H_2O	89	50,000	204	8,800	189
Ce	0.52	500	1.67	116	1.73
Pb	0.027	28	0.091	11	0.14
Sr	8.9	4000	18.1	1740	26.5
Sm	0.23	35	0.31	30	0.53
Yb	0.58	0	0.58	0	0.58
B*	0.12	400	1.03	-	-
$^{87}Sr/^{86}Sr$	0.70239	0.7090	0.70575	0.7035	0.70314
$^{206}Pb/^{204}Pb$	18.217	17.6	17.782	17.6	17.47
δD_{SMOW} (‰)	-679.9	-68	-68.8	-125	-98.7
$\delta^{11}B$ (‰)	-6.39	-6.6	-6.4	-	-
Ba/Nb	2.69	17.7	14.7	12	9.29
Ba/La	3.03	20.2	16.7	13	10.2
H_2O/Ce	171	100	122	76	109
H_2O/La	458	150	214	156	271
$(La/Sm)_N$	0.55	6.09	1.99	1.2	0.95
Ce/Pb	19.2	17.8	18.3	15	12.6
CO_2/Nb	486	267	289	293	330
CO_2/H_2O	0.93	2.0	1.53	2.0	1.5
CO_2/Ba	141	15.0	19.8	24	37
Cl/H_2O	0.038	0.037	0.033	0.038	0.034

Table S4-2
Table 3: Mineral and Bulk Distribution Coefficients (cont.)

Element	Splhrz	Gtlhrz (1%gt)	Gtlhrz (5%gt)
Ba	0.00012	0.00013	0.00015
Nb	0.0034	0.0040	0.0050
Cl*	0.0050	0.0055	0.0072
La	0.0070	0.0075	0.090
H_2O*	0.0086	0.011	0.013
Ce	0.010	0.011	0.014
Pb	0.014	0.017	0.020
Sr	0.025	0.027	0.030
Sm	0.040	0.055	0.65
Yb*	0.12	0.22	0.35

Bulk distribution coefficients for various mineral assemblages were calculated using the above mineral distribution coefficients of *Salters et al.* [2002], *Aubaud et al.* [2004], and *Workman and Hart* [2005].
* indicates elements whose distribution coefficients were obtained using interpolation.

Table S5-1: List of Acronyms

α – Stable isotopic fractionation factor between two substances, A and B, defined as
$\quad$ $\alpha_{A\text{-}B} = R_A/R_B = (\delta_A+1000)/(\delta_B+1000)$
C – Common mantle component
DampEM – EM-type end-member for southern Atlantic basalts
DMORB – Depleted Mid-Oceanic Ridge Basalt end-member
DMM – Depleted MORB mantle source
DryEM – EM-type end-member for northern East Pacifc Rise basalts
δX – del notation, where δX is the parts per thousand (permil) deviation from a standard. For
$\quad$ example, δD is the permil deviation of the D/H isotope ratio from the D/H ratio of Standard
$\quad$ Mean Ocean Water (SMOW), where $\delta D_{SMOW} = 0$ ‰.
EM – Enriched Mantle source (EM1 and EM2 referred to as EM)
EMORB – Enriched Mid-Ocean Ridge Basalt
EMP – Easter Microplate
EPR – East Pacific Rise
ESC – Easter Salas y Gomez Seamount Chain
FOZO – Focus Zone
FTIR – Fourier Transform Infrared Spectroscopy used for H_2O and CO_2 analysis
HIMU – "high μ, where $\mu = {}^{238}U/{}^{204}Pb$
HREE – Heavy Rare Earth Elements (e.g., Tm, Yb, Lu)
HSFE – High Field Strength Elements (e.g., Nb, Ta, Zr)
JM2 – Jan Mayen PREMA + EMI-type component defined by most enriched basalt composition
JM1 - Jan Mayen PREMA-type component defined by intersection of Mohns-Jan Mayen array
with NADM-Azores Platform array
LILE – Large Ion Lithophile Elements
LLSVP – Large low-shear-velocity provinces that form the ultra low velocity zone structures at
$\quad$ bottom of the core-mantle boundary
LREE – Light Rare Earth Elements (e.g., La, Ce, Pr, Nd)
MAR – Mid-Atlantic Ridge
MORB – Mid-Ocean Ridge Basalt
NADM – Northern Atlantic Depleted Mantle
NMORB – normal MORB, where enrichments in incompatible elements in
$\quad$ DMORB<NMORB<EMORB
OIB – Ocean Island Basalt
PacDM – Pacific Depleted Mantle
PAR – Pacific-Antarctic ridge 41° to 65°S
PHEM – Primitive Helium Mantle
PREMA – Prevalent Mantle enriched component
REE – Rare Earth Elements
SCLM – Sub-Continental Lithospheric Mantle
SYG – Salas y Gomez plume end-member as defined by most enriched basalt compositions
SYG* - C-H-O-Cl fluid PREMA-type mixing end-member involved in SYG mantle formation
SMOW – Standard Mean Ocean Water (SMOW), where $\delta D_{SMOW} = 0$ ‰.
TC/EA – Thermal Conversion Elemental Analyzer used for H_2O and δD_{SMOW} analysis
WetEM – C-O-H-Cl fluid EM-type end-member for Arctic Ridge basalts